Loss of endogenous tau suppresses APOE4-induced patterned behavioral decline and axon dysmorphia in a *C. elegans* model of Alzheimer's disease

Eric A. Cardona[1], Chelsea J. Webber[1], Zheng Wu[1], Blythe M. Bolton[2], Elif Sarinay-Cenik[2], Jonathan T. Pierce[1]

[1]Department of Neuroscience, Center for Learning and Memory, University of Texas at Austin, Austin, TX

[2]Department of Molecular Biosciences, University of Texas at Austin, Austin, TX

* For correspondence: jonps@utexas.edu

ORCID for Eric A. Cardona: 0000-0001-8003-2691

ORCID for Chelsea J. Webber: 0000-0002-7715-2278

ORCID for Jonathan T. Pierce: 0000-0002-9619-4713

Abstract

Alzheimer's disease (AD) causes a characteristic spatiotemporal pattern of neurodegeneration, resulting in the loss of associated faculties such as cognition. The factors that account for this pattern of degeneration are unclear, as AD risk genes are numerous and often broadly expressed. Previously, we generated a model of AD using the nematode *Caenorhabditis elegans* in which the AD risk variant of apolipoprotein E, *APOE4*, is pan-neuronally expressed. We showed that HSN class motor neurons degenerate in early adult stage animals. Here, we expand on our past work by performing behavioral analyses to deduce the effect of APOE4 on the function of distinct neuronal circuits. We found evidence that APOE4 induces dysfunction of other neurons; this spatiotemporal pattern roughly correlates with endogenous levels of PTL-1, the *C. elegans* homolog of human MAPT also known as tau. Moreover, deletion of *ptl-1* suppressed defects in multiple behaviors, suggesting broad protective effects across the nervous system including the HSN neurons. Lastly, we show that PTL-1 in the touch receptor neurons, where PTL-1 is most abundant, contributes non-cell autonomously for age-related

axon dysmorphia and dysfunction of the HSN neurons. Our results suggest that *C. elegans* may provide a useful *in vivo* system to study how endogenous Tau acts downstream of APOE4 to cause progressive, patterned neurodegeneration.

Introduction

Neurodegenerative disorders such as Alzheimer's disease (AD), Parkinson's disease (PD), and frontotemporal lobar dementia (FTLD) present with characteristic spatiotemporal patterns of neuronal cell death (Braak and Braak, 1991; Bahia et al., 2013; Reviewed in Rietdijk et al., 2017). Degeneration in characteristic brain regions corresponds to loss of brain region-associated faculties, such as memory in AD (Rosen et al., 2005). Genetic risk factors have been previously associated with AD. Among them, the ε4 variant of Apolipoprotein E (APOE4) is the most common genetic risk factor for earlier onset and faster progression of sporadic AD and AD-like pathology in individuals with Down syndrome (Larsen et al. 2024; Serrano-Pozo et al., 2021). A recent study proposed that *APOE4* homozygosity itself may be a single-gene driver of AD, akin to mutation of the familial AD genes *APP*, *PSEN1*, and *PSEN2* (Fortea et al., 2024; Ryan and Rossor, 2010). Moreover, APOE4 has been shown to increase the severity of other neurodegenerative diseases such as PD and FTLD (Robinson et al., 2018; Koriath et al., 2019; Davis et al., 2020). How APOE4 worsens neurodegeneration (as in AD, PD, and FTLD) or, more interestingly, may induce it (as suspected in AD) and contribute to patterned degeneration is unclear.

As *APOE4* homozygosity alone may cause AD, it is critical to understand how APOE4 contributes to patterned neurodegeneration. One hypothesis is APOE4-induced neurodegeneration follows a spatiotemporal pattern determined by cellular levels of specific vulnerability factors. Multiple lines of evidence suggest that the microtubule associated protein gene, *MAPT*, which encodes tau, represents one such vulnerability factor. First, pathogenic tau forms intracellular aggregates, and their accumulation is closely linked to neuronal dysfunction in AD and other degenerative disorders termed tauopathies (Trojanowski et al., 1993; Lin et al.,

55 2019). Second, tau-related pathology is highly correlated with neurodegeneration according to
56 Braak Staging, a well-established metric of how AD progresses with age (Braak and Braak,
57 1991; Köpke et al., 1993; Ghoshal et al., 2002). Third, transgenic expression of pathological tau
58 is sufficient to cause neurodegeneration (Mocanu et al., 2008; Spittaels et al., 1999;
59 www.alzforum.org/research-models). Fourth, depletion of endogenous tau mitigates cellular
60 correlates of AD pathology in rodent models of AD that overexpress human *APP* (Roberson et
61 al., 2007; Vossel et al., 2010) or human tau with aggregate-inducing mutations (Wegmann et al.,
62 2015; DeVos et al., 2017). Fifth, growing evidence suggests that pathogenic tau protein can
63 spread in a trans-synaptic fashion between brain regions *in vivo* with age (Liu et al., 2012; de
64 Calignon et al., 2012; Iba et al., 2013; Fu et al., 2016; Meisl et al., 2021; Cornblath et al., 2021).
65 Altogether, these and many other studies provide strong evidence for tau as a candidate
66 vulnerability factor underlying patterned neurodegeneration. Progress has been made to
67 uncover the relationship between APOE4, tau, and neurodegeneration (Shi et al., 2017;
68 Therriault et al., 2020; Seo et al., 2023; Koutsodendris et al., 2023), but whether APOE4 is a
69 causative factor in the pathogenic spread of tau or how APOE4 may contribute to a combination
70 of cell autonomous and non-cell autonomous processes is less clear. Additionally, because
71 rodent models of AD often do not fully recapitulate the neurodegeneration observed in human
72 patients, the cellular molecular bases for this critical pathological phenotype remain have yet to
73 be uncovered.
74 The nematode *Caenorhabditis elegans* has been famously leveraged to discover
75 conserved *in vivo* mechanisms of cell death (Horvitz, 2003). It also represents a potentially
76 useful system to study the cellular molecular bases for patterned neurodegeneration *in vivo*. To
77 model neurodegeneration, past studies have overexpressed human disease genes and
78 investigated the health and function of specific neurons *in vivo* (Faber et al., 1999; Baskoylu et
79 al., 2018; van Ham et al., 2008; Vaccaro et al., 2012b). In transgenic *C. elegans* models,
80 progress has been made to investigate genes involved with AD, notably *MAPT* and *APP*
81 (Kraemer et al., 2003; Treusch et al., 2011; Fatouros et al., 2012; Benbow et al., 2020; Sae-Lee

et al., 2020). A powerful feature of *C. elegans* as a model organism is that each one of its 302 neurons is identifiable. However, previous studies did not take full advantage of this to investigate whether specific neurons differ in vulnerability due to tau. Thus, the potential of *C. elegans* to test spatiotemporal patterns of neurodegeneration remains underutilized.

Here, we found that APOE4 induces a spatiotemporal pattern of behavioral decline in *C. elegans* as inferred through the assessment of behaviors that reflect the activity of known neurons. This pattern roughly correlates with neuronal expression levels of *ptl-1*, the sole worm ortholog of *tau*. Complementing our indirect approach, we observed directly via live microscopy that APOE4 induces progressive, age-related HSN axon dysmorphia coincident with dysfunction of that neuron. Deletion of *ptl-1* suppressed both APOE4-induced behavioral defects and HSN axon dysmorphia. Genetic ablation of the six neurons most enriched with PTL-1—the touch receptor neurons (TRNs)—similarly suppressed HSN dysfunction; this was phenocopied by targeted depletion of PTL-1 in the TRNs. These results suggest a non-cell autonomous role for PTL-1 in APOE4-induced degeneration. Overall, our findings position the APOE4 worm model as a useful system to study how endogenous tau/PTL-1 participates in the cellular molecular mechanisms underlying patterned neuronal dysmorphia or degeneration. This may aid in the development of new therapeutic measures against tauopathies, such as AD.

Results

APOE4 induces progressive, widespread behavioral defects in *C. elegans*

Our previous study using *C. elegans* showed that pan-neuronal expression of *APOE4* induced degeneration of a subset of neurons (the HSN pair) in early adult, while others (such as VA and VB class neurons) appeared to remain healthy (Sae-Lee et al., 2020). To expand on this study, we investigated whether APOE4 induces a wider pattern of neurodegeneration. We assayed a variety of behaviors to assess the function of different subsets of neurons. We reasoned that we

108 could deduce the health and function of different neuronal subsets and circuits by measuring the
109 performance of these behaviors.

110 We selected seven different behaviors that rely primarily, but not exclusively, on mostly
111 distinct subsets of identified neuron classes (Fig. S1). Five behaviors we tested—*egg laying*,
112 *pharyngeal pumping*, *gentle* and *harsh touch response*, and *locomotor gait transition*—have
113 specific neurons that are critical for behavioral execution. These include: the HSN class neurons
114 for egg laying behavior (Schafer, 2005); the MC and M3 neurons for pumping of the pharyngeal
115 feeding organ (Avery and You, 2012); the six touch receptor neurons (TRNs) for gentle touch
116 response (Chalfie and Sulston, 1981; Chalfie et al., 1985); the FLP and PVD neurons, with
117 lesser contribution from redundant mechanoreceptive neurons and interneurons, for harsh touch
118 response (Li et al., 2011); and lastly, the ADE and PDE dopaminergic neurons for the transition
119 between swim and crawl locomotor gaits (Vidal-Gadea et al., 2011). We also assessed two
120 readouts of locomotor behavior that rely on many more neurons with partial redundancy. *Short-*
121 *term locomotion* relies on over 100 motor neurons and about one dozen pre-motor interneurons;
122 *long-term locomotion* relies on those neurons and additional sensory neurons and interneurons
123 to mediate switches between roaming and dwelling states (Flavell, et al., 2020).

124 We evaluated behavioral performance at adult days 1 through 5 (D1-5) (Fig. 1A left).
125 This age range encompasses the peak reproductive period when *C. elegans* is active across a
126 range of behaviors and lays eggs (Scharf et al., 2021). We refer to “age of onset” of behavioral
127 decline as the first day of the adult stage that APOE4 worms displayed significantly impaired
128 behavior compared to age-matched controls.

129 Over the course of D1-5 of adult, we found that APOE4 worms displayed differences in
130 all seven behaviors compared to control (Fig. 1B-H). In as early as D1 adults, gentle touch
131 sensitivity, pharyngeal pumping, and short-term locomotion performances decreased by 11%,
132 13%, and 24%, respectively; gait transition decreased by a marked 59% (Fig. 1B-E). In D2
133 adults, long-term locomotion showed a 12% decline. We also replicated our previous finding of
134 an egg-laying defect that leads to larvae hatching internally, a salient phenotype called

135 “bagging” (Sae-Lee et al., 2020; Fig. 1G). APOE4 worms showed a salient 60% incidence of
136 bagging, peaking at D3. Whereas other behavioral performances declined, harsh touch
137 sensitivity oddly increased in APOE4 worms relative to control beginning at D3 (Figs. 1H, S2).
138 Altogether, these results indicate that APOE4 induces age-related abnormalities in multiple
139 behaviors that primarily rely on distinct subsets of neurons. Thus, the APOE4 worm exhibits a
140 wider spatiotemporal pattern of neuronal dysfunction, beyond the HSN neuron pair, across early
141 worm adult age.

142 The APOE4 worm exhibited a few defects in behaviors as early as D1 adult. To test
143 whether this represents a defect that originates during or after development we evaluated gentle
144 touch and pumping behaviors in L4 stage worms (~24 hours younger than D1 adults) out to D3
145 of adulthood for a new set of worms (Figs. 1A left, 2). A two-way ANOVA was used with planned
146 pairwise comparisons. Gentle touch and pumping behavior did not statistically differ between
147 control and APOE4 groups (compare L4 timepoints in Fig. 2A to 2B and 2C to 2D). Throughout
148 adult stage, gentle touch remained unchanged as expected into D1 and D3 for control (Pan et
149 al., 2011), whereas sensitivity decreased in APOE4 ($p<0.02$). In contrast, while pumping rate in
150 control worms increased as expected from L4 to D1 ($p<0.05$; Hosono et al., 1980; Huang et al.,
151 2004; Fig. 2C), the rate remained unchanged in APOE4 worms (Fig. 2D). Thus, there likely exist
152 mixed or multiple mechanistic underpinnings of APOE4-induced behavioral decline, such as
153 age-related decline (as with gentle touch) or developmental defects (as with pharyngeal
154 pumping).

155

156 **APOE4-induced progressive behavioral defects depend on the worm ortholog of tau**

157 Above, we reported that gentle touch response is among the first behaviors to decline
158 with APOE4 on D1 adult. This behavior is mediated by the six touch receptor neurons (TRNs)
159 that feature a prominent array of microtubules that were exploited to discover the first
160 microtubule gene (Chalfie and Thomson, 1979; Chalfie and Thomson, 1982). Studies have
161 shown that tau binds to and stabilizes neuronal microtubules in mammals (Butner and

162 Kirschner, 1991; Santarella et al., 2004). As one may expect from microtubule-enriched
163 neurons, the worm homolog of tau, PTL-1, is highly enriched in the TRNs compared to other
164 neurons, notably the PLM and ALM classes, according to recent single-cell transcriptomic
165 analyses (Taylor et al., 2021; Roux et al., 2023; Fig. S3 green bars). We also noticed a rough
166 correlation between endogenous levels of PTL-1 in specific neurons across the nervous system
167 and the age of onset for APOE4-induced behavioral decline. This is depicted in Fig. S1, where
168 gray shows what fraction of *ptl-1* is expressed in critical neurons that subserve each behavior.
169 Given that tau represents a pathological hallmark associated with neurodegeneration in AD, we
170 speculated that the high endogenous levels of PTL-1 in the TRNs may explain the early onset
171 for the APOE4-induced gentle touch defect. Following this idea, we also hypothesized that
172 deletion of *ptl-1* may broadly confer neuroprotection against APOE4. Into an APOE4
173 background we crossed a *ptl-1* mutant bearing the *ok621* deletion allele (Δ*ptl-1*). This allele
174 represents a strong hypomorph, if not a null allele, as it lacks four exons that encode conserved
175 microtubule-binding domains important for PTL-1 function (Goedert et al., 1996; Gordon et al.,
176 2008; Hashi et al., 2015; Figs. 1A right, S4).

177 We found that deletion of *ptl-1* significantly suppressed APOE4-induced defects in four
178 out of seven behaviors. Defects in gentle touch and pharyngeal pumping were completely
179 suppressed (Fig. 1B,C), while defects in gait transition and egg laying were partly suppressed
180 (Fig. 1D,G). We did not observe suppression of APOE4-induced abnormalities in short- and
181 long-term locomotion nor for harsh touch sensitivity (Fig. 1E,F,H). As a control, we found that
182 the *ptl-1* mutant was indistinguishable from control for six out of seven behaviors. Although the
183 *ptl-1* mutant displayed a moderate defect in swim-to-crawl transition compared to control, the
184 *ptl-1* mutant nonetheless partially suppressed the defect induced by APOE4 as opposed to
185 additively worsening the defect (Fig. 1D). Also, although *ptl-1* mutant displayed a non-significant
186 trend toward lower bagging compared to control animals, it significantly suppressed APOE4-
187 induced bagging (Fig. 1G).

188 Altogether, we conclude that PTL-1 variably contributes to the neuronal dysfunction
189 given multiple significant behavior changes induced by APOE4.
190
191 **APOE4-induced degeneration of HSN axon requires worm ortholog of tau**
192 Previously, we showed that APOE4-induced bagging coincided with degeneration of the
193 bilaterally symmetric pair of HSN egg-laying motor neurons (Sae-Lee et al., 2020). Because
194 deletion of *ptl-1* suppressed APOE4-induced bagging, we hypothesized that *ptl-1* deletion would
195 also suppress HSN degeneration. To test this, we inspected the health of reporter-labeled HSN
196 neurons in live worms with epifluorescent microscopy. Dorsal to the vulva, which is the egg-
197 laying orifice, the HSNs are situated in the midbody of the worm (depicted in Fig. 3A). To
198 quantify degeneration, we initially calculated various metrics of HSN soma geometry and
199 reporter intensity across strains (Fig. S5A), focusing on D3 adult animals which is the age of
200 onset for increased bagging (~70% incidence in APOE4 worms; Figs. 1G, 3E).
201 Consistent with our previous study (Sae-Lee et al., 2020), we found that the HSN soma
202 appeared on average much dimmer in APOE4 than control worms, indicative of degeneration
203 (Fig. S5D). However, deletion of *ptl-1* alone also appeared to have caused dimming along with
204 abnormally large appearance of the HSN soma (Fig. S5B,D). We found no straightforward
205 relationship between other soma morphometrics and HSN dysfunction as reflected by bagging
206 incidence across control, *ptl-1*, and APOE4 strains (compare Fig. 1G to Fig. S5 measures).
207 Thus, we conclude that HSN soma geometry and brightness are inconsistent predictors of HSN
208 function in these strains, possibly due to unforeseen aspects of the fluorescent reporter (see
209 Methods).
210 Seeking a more reliable cellular correlate of HSN function, we next investigated HSN
211 axon morphology. Previous work using laser ablation and mutants showed the proximal axon
212 portion (located between soma and vulval muscles)—but not distal portion which continues
213 anteriorly—is required for egg laying behavior (Garriga et al., 1993; Fig. 3A). Therefore, we

214 hypothesized that morphology of the proximal axon may serve as a useful correlate of HSN
215 neuron function.
216 We visualized the HSN proximal axon with the same fluorescent reporter as above for
217 the soma. The ~11 µm-long HSN proximal axon typically comprises two segments joined at a
218 right-angle (Fig. 3B image 1). The initial segment, which is qualitatively thicker, projects
219 anteriorly from the soma (segment i.) before turning ventrally at a right-angle into a second,
220 thinner segment (segment ii.) that joins the ventral nerve cord (VNC) and branches dorsally to
221 innervate egg-laying musculature. The unbranched, distal axon continues anteriorly within the
222 VNC to the head (Fig. 3A; Garriga et al., 1993). In our control reporter strain, we found that
223 ~58% of worms had a proximal axon with this typical two-segment, right-angle morphology
224 (N=93; Fig. 3B image 1), while the remainder had a single ventrally-projecting proximal axon
225 from the soma (Fig. 3B image 2). The latter single-segmented axons were thin and resembled
226 segment ii. of two-segment HSN proximal axons. We speculate that the thicker, anteriorly
227 directed segment i. did not develop in these worms because the HSN soma had already
228 migrated to a position directly dorsal from the vulval muscles. Although the HSN proximal axon
229 has been previously depicted with two segments connected at a right angle (Asakura et al.,
230 2007; Tsutsui et al., 2021), both configurations have been described in the literature and are
231 functional (Garriga et al., 1993). Thus, both types of proximal axons were scored as normal.
232 To check for axon abnormalities potentially caused by APOE4, we next qualitatively
233 scored the morphology of HSN proximal axons and quantified their lengths in D3 adult animals.
234 We found that the incidence of abnormal proximal axons was more than double in APOE4
235 compared to control worms. Proximal axons often took eccentric, elongated paths in APOE4
236 worms (compare Fig. 3B normal images 1,2 to abnormal images 3-10). This was not easily
237 explained by abnormal positioning of the HSN soma, as the somas were similarly located in
238 both APOE4 and control worms; soma positions were quantified as the HSN soma to VNC
239 distance and the HSN soma to vulva area distance (Fig. S6C left) or the angle formed between
240 these two vectors (Fig. S6C right; Asakura et al., 2007).

241 We observed at least three distinct qualitatively abnormal morphologies of the proximal
242 axons relative to control. First, segment i. (Fig. 3B, image 3) or segment ii. (Fig. 3B, image 4)
243 had an extra ~90-degree turn. Second, segment i. connected to segment ii. with a typical right-
244 angle turn, but displayed an atypical ~45-degree portion, with an apparently wider segment near
245 the soma (Fig. 3B images 5,6). Third, segments i. and ii. together took on a hook-like shape
246 oriented anteriorly (Fig. 3B images 7,8). We also noted additional cases (<5% frequency) where
247 these morphological abnormalities appeared to co-occur (e.g., segment ii. extra right-angle turn
248 and segment i. 45-degree portion, Fig. 3B, image 10). Overall, we conclude that APOE4
249 appears to induce a variety of proximal axon abnormalities of the HSN neurons.
250 To help distinguish whether the HSN proximal axon abnormality represented a
251 developmental defect, age-related degeneration, or both, we inspected younger adult animals to
252 determine when the defect started. In D1 adults, there was a no significant difference in the
253 incidence of abnormal axons in APOE4 worms versus control (Fig. 3C). However, in D3 adults,
254 the incidence of abnormal axons showed a three-fold increase in APOE4 worms versus control
255 (Fig. 3D). Additionally, at the even younger L4 developmental stage, the entirety of HSN axon
256 appears to project properly in ~95% of APOE4 animals (Fig. S7B). From these observations, we
257 deduce that the proximal axon defect begins by at least D1 in some APOE4 worms and
258 progresses in an age-related fashion, concurrent with the age of onset for increased bagging
259 and with similar incidence (Fig. 3G). We thus conclude that the increased incidence in axon
260 abnormality likely reflects a degenerative phenotype.
261 We next tested whether deletion of *ptl-1* might suppress APOE4-induced abnormal HSN
262 proximal axon morphology. To partly control for genetic background, we inspected two
263 independent isolates of APOE4;Δ*ptl-1* worms that were crossed with the HSN reporter strain.
264 For both isolates, we found that the *ptl-1* deletion suppressed the APOE4-induced abnormal
265 axon morphology (Fig. 3D).
266 The similar incidence of axon abnormality and bagging in APOE4 worms led us to
267 conclude that abnormal proximal axons reflect a defect in HSN function (compare control to

268 APOE4 in Figs. 1G, 3D,E). This is bolstered by our observation that deletion of *ptl-1* suppresses
269 APOE4-induced defects in behavioral performance as well as HSN proximal axon morphology.
270 Altogether, the above results support the idea that proximal HSN axon morphology is a reliably
271 predictive correlate of efficient egg-laying behavior and thus HSN health and function.
272
273 **Ablating tau-rich touch receptor neurons protects HSN from APOE4-induced dysfunction**
274 The spatiotemporal pattern of degeneration in AD is thought to be partly explained by
275 pathological forms of tau spreading between connected neurons and across the brain (intra-
276 and extra-synaptically; Liu et. al, 2012; de Calignon et al., 2012). As shown above, the systemic
277 deletion of *ptl-1* protected against age-related APOE4-incuded behavioral defects and abnormal
278 HSN proximal axon morphology. We next sought to test whether PTL-1 might contribute non-
279 cell autonomously to degeneration, explaining in part the spatiotemporal pattern of behavioral
280 decline in our APOE4 worm model. We hypothesized that targeting the neurons that are 1) most
281 abundant with PTL-1, and 2) tend to become dysfunctional early, may suppress the subsequent
282 degeneration of other neurons that express PTL-1 at a lower level. The TRNs represent the
283 neuronal class most abundant in PTL-1 in *C. elegans*. Over 30% of neuronal *ptl-1* transcripts
284 are expressed in the mere six TRNs (Figs. S1,S3 green bars; Taylor et al., 2021; Roux et al.,
285 2023). Coincidentally, the TRNs also become dysfunctional in D1 adults (Fig. 1B). In contrast,
286 the HSN neurons express ~80% less *ptl-1* than the TRNs and become dysfunctional later
287 starting in D3 adults (Figs. 1G,S3 blue bar; Taylor et al., 2021). Some TRNs are also nearby the
288 HSN neurons, such as the PLMs which synapse onto the HSN neurons (White et al., 1986).
289 Thus, the TRNs and HSN neurons in worm offer a convenient platform to test whether PTL-1
290 contributes non-cell autonomously to degeneration.
291 To assess the TRNs and PTL-1 protein *in vivo* during our targeted manipulations, we
292 took advantage of a control strain in which endogenous PTL-1 protein is translationally tagged
293 with mNeonGreen (PTL-1::mNG; Krieg, et al., 2017). Consistent with transcriptional studies,
294 TRNs were readily visible in living larval and adult stages by their abundant mNG-tagged PTL-1

295 (Representative PLM neuron in Figs. 4A2, 5B2). We also tested whether the mNG tag on PTL-1
296 impedes its apparent neurotoxic properties downstream of APOE4. If this were the case, we
297 might expect less HSN dysfunction in APOE4;PTL-1::mNG worms. Instead, we found bagging
298 incidence in APOE4;PTL-1::mNG worms (60%) was similar to that of the APOE4-alone strains
299 generated in the current (~70%) and our previous (50-60%) studies (note: all APOE4 strains
300 depicted in Fig. 4A1 express mNG::PTL-1, versus those in Fig. 1G which do not; Sae-Lee et al.,
301 2020). We conclude that the endogenous mNG tag does not interfere with the presumed toxicity
302 of PTL-1 in an APOE4 background.

303 For our first targeted manipulation, we tested whether ablation of the TRNs suppresses
304 APOE4-induced HSN dysfunction. To do this, we leveraged the apoptotic trigger EGL-1, the
305 sole worm homolog of the human BH3-only domain proteins BAM and BID. Targeted
306 expression of *egl-1* has been previously used to kill specified cells (Chang et al., 2006). To kill
307 the TRNs, we generated a strain whose *egl-1* expression is driven by the promoter of *mec-17*, a
308 gene expressed exclusively in the TRNs (TRNs::EGL-1; Wu et al., 2025). The TRNs::EGL-1
309 strain was then crossed into the mNG-tagged *ptl-1* genetic background. To confirm the efficacy
310 of TRN genetic ablation, we took advantage of the relative abundance of mNG-tagged PTL-1 in
311 the TRNs (Fig. S3 green bars), which could be directly observed using epifluorescence
312 microscopy (Fig. 4A2 control). Anatomically, this was easier to test with the PLM class of TRNs
313 due to how its soma and process are confined in the narrow tail region, in contrast with the other
314 TRN classes with soma situated in the thicker midbody (Fig. 4A2 control; WormAtlas). We found
315 that 93% of TRNs::EGL-1 animals had no detectable PTL-1::mNG where PLM soma and
316 processes were expected compared to control (N=46; Fig. 4A2), suggesting a successful cell
317 ablation in most cases.

318 We found that ablating the TRNs partially suppressed APOE4-induced HSN dysfunction
319 as indicated by a ~30% reduction in bagging incidence (Fig. 4A1 yellow bar). Ablation of the
320 TRNs alone in the control strain had no effect on bagging (Fig. 4A1 white bar). Impressively,
321 ablating the TRNs conferred a similar magnitude of protection as afforded by systemic deletion

322 of *ptl-1* (compare blue bar in Fig. 1G to yellow bar in Fig. 3A1). Thus, we deduce that TRNs
323 activity and/or their cellular contents may contribute non-cell autonomously to APOE4-induced
324 HSN degeneration.

325 Because TRN activity is obviously lost after genetic ablation, we asked whether simply
326 blocking TRNs function alone as opposed to whole cell ablation may protect the HSNs against
327 APOE4. We tested this by using a deletion allele of *mec-4*, a gene that encodes
328 mechanoreceptive DEG/ENaC channel expressed predominantly in the TRNs (Chalfie and
329 Sulston, 1981). We took advantage of the *u253* loss-of-function allele of *mec-4*, referred hereon
330 as *mec-4*(*lf*), abolishes transduction of mechanosensory currents and gentle touch response yet
331 leaves the TRNs otherwise physiologically and morphologically normal (O'Hagan, et al., 2005).
332 We found that *mec-4*(*lf*) failed to suppress APOE4-induced HSN dysfunction (Fig. 4B). From
333 this, we conclude that functional impairment of the TRNs is insufficient to protect HSNs against
334 APOE4.

335 **Targeted reduction of tau in touch receptor neurons protects HSN against APOE4**

336 Because the worm ortholog of tau, PTL-1, is especially abundant in the TRNs (Fig. S3
337 green bars), we hypothesized that targeted depletion of PTL-1 contained in the TRNs would
338 protect against APOE4-induced HSN dysfunction, phenocopying TRNs ablation. To test this, we
339 knocked down *ptl-1* expression in the TRNs using cell-selective RNAi as previously described
340 (TRNs::*ptl*-1 KD; Esposito et al., 2007). To determine the efficacy and selectivity of the
341 knockdown, we quantified PTL-1::mNG fluorescence intensity in TRN soma versus example
342 non-targeted neurons. Conveniently, the soma of the non-targeted VC4 and VC5 class motor
343 neurons are also easily detectable by PTL-1::mNG fluorescence (Fig. 3A blue neurons; Fig. S3
344 blue bars). Compared to control, TRNs::*ptl-1* KD worms had an average 40% decrease in PTL-
345 1::mNG fluorescence in five out of the six TRNs (Fig. 5A2). In contrast, PTL-1::mNG
346 fluorescence intensity was unchanged in the non-targeted VC4 and VC5 neurons (Fig. 5A2).
347 These observations suggested an effective and selective knockdown of *ptl-1* in the TRNs.

348 Using this strategy, we found that knockdown of *ptl-1* in the TRNs partially suppressed
349 APOE4-induced HSN dysfunction. This was determined after scoring bagging in two
350 independent isolates of APOE4 worms crossed with the TRNs::*ptl-1* KD strain to partly control
351 for genetic background (Fig. 5A1 blue bars). In contrast, knockdown of *ptl-1* in TRNs alone in
352 the control strain had no effect on bagging (Fig. 5A1 white bar). While significant, the
353 suppressive effect was noticeably weaker compared to the systemic *ptl-1* deletion (compare
354 with APOE4;Δ*ptl-1* strain, blue bar in Fig. 1G). We speculated that the weaker suppression may
355 be explained by RNAi reducing only a portion of *ptl-1* transcripts in the TRNs (Fig. 5A2). This
356 prompted us to test whether complete loss of *ptl-1* in the TRNs more strongly suppresses HSN
357 dysfunction than in APOE4;TRNs::*ptl-1* KD worms.
358 To achieve a targeted *ptl-1* knockout in the TRNs, we used an intersectional Cre-LoxP
359 approach. *LoxP* sites were first introduced via CRISPR to flank the endogenous *ptl-1*::*mNG*
360 locus (*LoxP*::*ptl-1*::*LoxP* strain). *LoxP*::*ptl-1*::*LoxP* worms were then crossed with a strain that
361 expresses Cre recombinase under the same TRNs-specific promoter as our TRNs::EGL-1 strain
362 (Harterink et al., 2018; Sanfeliu-Cerdán et al., 2023; Wu et al., 2025). This should result in a
363 selective knockout of *ptl-1* in the TRNs (TRNs::*ptl-1* KO). The efficacy of the *ptl-1* knockout was
364 confirmed by evaluating the presence of PTL-1 in the PLM neurons via PTL-1::mNG
365 fluorescence signal (Fig. 5B2). PTL-1::mNG was absent in 100% of PLM neurons in TRNs::*ptl-1*
366 KO animals (N=45). Evaluation of protein by Western blot with the FLAG epitope on the tag
367 using whole-animal lysate was inconclusive due to high variability (Fig. S8; Krieg et al., 2017).
368 As with the knockdown, we found that knockout of *ptl-1* in the TRNs partially suppressed
369 APOE4-induced HSN dysfunction. This was determined after scoring bagging in two
370 independent isolates of APOE4 worms crossed with the TRNs::*ptl-1* KO strain to partially control
371 for genetic background (Fig. 5B1 blue bars). In contrast to the mild suppression after *ptl-1*
372 knockdown (Fig. 5A1 blue bars), the average extent of suppression by knockout in the TRNs
373 was more equivalent to that of the systemic deletion of *ptl-1* (Fig. 1G).

374 Finally, we inspected HSN axons directly to test whether knockout of *ptl-1* in the TRNs
375 suppresses APOE4-induced abnormal morphology. To do this, we generated new transgenic
376 reporter lines using our TRNs::*ptl-1* KO and APOE4;TRNs::*ptl-1* KO strains (Fig. 5B1 white and
377 left blue bar). In these strains, we observed no difference in the incidence of abnormal HSN
378 proximal axons comparing the no-APOE4 control to the APOE4 worms (Fig. 5B3). We conclude
379 that knockout of *ptl-1* in the TRNs is sufficient to suppress the axon morphology defects induced
380 by APOE4.
381 Does loss *ptl-1* in neurons other than the TRNs suppress APOE4-induced HSN
382 dysfunction? Aside from the TRNs, other sensory neurons in *C. elegans* are also abundant in
383 tau/PTL-1. These include a subset of over two dozen neurons that express the intraflagellar
384 transport protein CHE-2 in the ciliary basal body (Fig. S3 yellow bars; Fujiwara et al., 1999;
385 Taylor et al., 2021). As with our strategy for the TRNs, we generated a strain in which *ptl-1* was
386 knocked out in the these sensory neurons by crossing our *LoxP*::*ptl-1*::*LoxP* strain a strain
387 whose Cre recombinase expression is driven by the *che-2* promoter (CHEs::*ptl-1* KO). We
388 observed no significant suppression in APOE4;CHEs::*ptl-1* KO compared to APOE4 alone (Fig.
389 5C), suggesting PTL-1 in the broad set of *che-2*-expressing sensory neurons is not required for
390 APOE4-induced HSN dysfunction.
391 Altogether, we conclude that PTL-1 in the TRNs contributes non-cell autonomously to
392 APOE4-induced dysmorphia of the HSN neuron axons. We do not conclude that TRNs
393 represent the only source of harmful tau.
394
395 **Discussion**
396 **APOE4-induced pattern of behavioral decline in *C. elegans***
397 In this study, we build on our prior work by characterizing APOE4-induced, age-related
398 abnormalities across seven behaviors in a *C. elegans* model of Alzheimer's disease (AD). The
399 pattern of decline provides evidence for spatiotemporal APOE4-induced neuronal dysfunction,

400 dysmorphia, and, perhaps, degeneration. Finally, we demonstrate that endogenous tau
401 contributes to APOE4-induced axon dysmorphia and multiple behavioral defects.
402 *C. elegans* has served as a leading model organism to study forms of cell death (Horvitz
403 2003); however, its potential to study *patterned neurodegeneration* in response to human
404 disease genes remains to be explored. This prompted us to ask whether APOE4 worms display
405 a pattern of neurodegeneration beyond the HSN neurons as we previously reported (Sae-Lee et
406 al., 2020). By day 4 (D4) of adulthood, APOE4 worms exhibit defects of varying severity in all
407 seven tested behaviors. Because each behavior primarily relies on mostly distinct subsets of
408 neurons (Fig. S1), this suggests a progressive, neuron-specific pattern analogous to the
409 characteristic progression observed in human AD (Braak and Braak, 1991; Scahill et al., 2002;
410 Fiford et al., 2018). The sensitivity of certain behaviors to decline merits follow up studies to
411 investigate putative higher-vulnerability neurons (e.g., the ADE and PDE neurons required for
412 swim-crawl gait transition; Fig. 1D; Vidal-Gadea et al., 2011). Certain behaviors were not
413 impacted by pan-neuronal APOE4 expression, perhaps indicating resilience to PTL-1-mediated
414 degeneration or dysfunction. This idea is mirrored in human AD where brain regions such as the
415 somatosensory cortex and brainstem are similarly spared from degeneration, even in advanced
416 stages of AD (Rondina et al., 2018). Alternatively, apparent resistance to APOE4 may reflect
417 neuronal circuit redundancy. In this vein, the subtle defects we observed in locomotion could
418 reflect the suspected functional redundancy of *C. elegans* motor neurons (Fig. 1E,F; Izquierdo
419 and Beer, 2018). Interestingly, harsh-touch sensitivity subtly *increased* in APOE4 worms, hinting
420 at neuronal hyperexcitability (Fig. 1H). In mouse, APOE4-driven hyperexcitability may result
421 from degeneration of inhibitory neurons (Nuriel et al., 2017a). This aligns with fMRI studies of
422 AD patients showing abnormally high activity in certain brain regions (Bookheimer et al., 2000;
423 Tuovinen et al., 2020). Future studies could explore how APOE4 alters excitability of harsh
424 touch neurons (e.g., the PVDs) and how this may correlate with APOE4-induced progressive
425 dysmorphia of the elaborate PVD dendrite arborization (Jiang et al., 2025).

426 Axon dysmorphia, or axonopathy, is a hallmark of human AD characterized by neurite
427 deterioration and general white matter abnormalities (Lee et al., 2016). Similar axon defects,
428 sometimes without cell body loss, have been observed in human AD patients and mouse
429 neurodegenerative disease models (Leroy et al., 2007; Yoshiyama et al., 2007; Crespo-Biel et
430 al., 2014). Here, we identified APOE4-induced dysmorphia of the HSN proximal axon (Fig. 3).
431 Our findings suggest this reflects a degenerative phenotype rather than a developmental defect
432 because: HSN soma appear to migrate appropriately (Fig. S6), full axons project as expected in
433 pre-adult L4 stage animals (Fig. S7), and the incidence and timing of abnormal axon
434 morphology in D1 versus D3 adult APOE4 worms closely follow the HSN-associated egg laying
435 defect (Figs. 1G, 3E). Worm neurons have been shown to contain axonal domains with distinct
436 structures and functions (Mizumoto and Shen, 2013; Eichel et al., 2022). Future studies should
437 consider what molecular factors might render the proximal HSN axon vulnerable to dysmorphia.
438 Overall, the tight correlation between a salient behavioral phenotype (bagging; Fig. 1G, 3G) and
439 axon dysmorphia of an identified neuron (HSN; Fig. 3) provides a powerful system to study
440 subcellular mechanisms of APOE4-induced axonopathy.
441 *C. elegans* has become increasingly recognized as a valuable *in vivo* model for studying
442 tau pathology (Reviewed in Natale et al., 2020). Along with extracellular amyloid-β plaques,
443 intracellular tau aggregation is a key pathological hallmark of AD (Kowall and Kosik, 1987; Kosik
444 et al., 1988; Grunke-Iqbal et al., 1986; Lee and Trojanowski, 1992). In AD and other
445 tauopathies, tau undergoes conformational changes that promote aggregation into tangles,
446 driving neurodegeneration (Friedhoff et al., 1998a,b; Jeganathan et al., 2006; Jeganathan et al.,
447 2008; Oakley et al., 2020). Unlike mammals, which have three broad tau-related gene families,
448 the worm has but a single endogenous homolog: *ptl-1* (Sündermann et al., 2016; Goedert et al.,
449 1996; Gordon et al., 2008). We found that deletion of *ptl-1* suppresses APOE4-induced defects
450 in four out of seven tested behaviors—including HSN-associated bagging—*and* HSN axon
451 morphological defects induced by APOE4. This fits with the idea that tau acts as an effector of
452 pathogenic events in AD initiated by APOE4. Indeed, past immunohistochemical evidence

453 suggested that APOE and tau co-localize – and possibly physically interact – in postmortem
454 brain tissue from individuals with Alzheimer's disease (Benzing and Mufson, 1995; Brecht et al.,
455 2004; Zhou et al., 2006; Rohn et al., 2012). Further studies showed that APOE4 expression
456 induces tau aggregates in cultured mouse neurons and worsens tau pathology in an AD mouse
457 model (Huang et al., 2001; Seo et al., 2023; Koutsodendris et al., 2023 Shi et al., 2017). It will
458 be interesting to see whether endogenous worm PTL-1 has similar pathological capacity
459 detectable at the biochemical level.

460 We found that deletion of endogenous *ptl-1* suppresses APOE4-induced axon
461 dysmophia. This parallels a previous report in a mouse AD model in which APOE4-induced
462 dysfunction of specific interneurons was suppressed by knocking out endogenous murine tau
463 (Andrews-Zwilling et al., 2010). Interestingly, another study found that depletion of endogenous
464 tau protected against neurodegeneration in an amyloid-β mouse model (Roberson et al., 2007).
465 Because *C. elegans* lacks an *APP* ortholog whose protein product is capable of generating
466 amyloid-β fragments (Daigle and Li, 1993), the benefits of PTL-1 reduction likely operate
467 independently of amyloid-β. Interestingly, a recent study found that *ptl-1* deletion partly mitigated
468 age-dependent accumulation of pathogenic human tau upon its overexpression in worm
469 neurons (Nunez et al., 2022). Thus, the APOE4 worm model of AD represents an Aβ-agnostic
470 model to investigate how endogenous tau contributes to patterned degeneration downstream of
471 APOE4.

472 PTL-1 may contribute non-cell autonomously to degeneration in our APOE4 worm
473 model. The touch receptor neurons (TRNs) contain the majority of PTL-1 in the worm nervous
474 system (Fig. S3 green bars; Taylor et al., 2021; Roux et al., 2023). We found that depleting
475 PTL-1 in the TRNs via genetic ablation, RNAi-mediated knockdown, and Cre-LoxP-mediated
476 knockout all partially suppressed APOE4-induced dysfunction of HSN neurons. Each targeted
477 manipulation roughly matched the magnitude of suppression achieved by systemic *ptl-1*
478 deletion. This raises the intriguing possibility that, although *ptl-1* remains widely expressed,
479 PTL-1 from the mere six TRNs is required non-cell autonomously for HSN dysfunction.

480 How might PTL-1 in the TNRs lead to APOE4-induced degeneration of the HSNs? The
481 popular hypothesis that pathological tau spreads across the brain offers a partial link between
482 tau pathology and spatiotemporal neurodegeneration (Braak and Braak, 1991; Reviewed in
483 Braak and Del Tredici, 2011; Frost et al., 2010). Studies with tauopathy mouse models have
484 shown that pathological tau can propagate across synapses, starting from "seed" regions rich in
485 Tau (and high in inter-neuronal connectivity) and spreading to distant brain regions (Clavaguera
486 et al., 2009; Kfoury et al., 2012; Liu et al., 2012; de Calignon et al., 2012; Iba et al., 2013).
487 Similarly, we hypothesize that pathological PTL-1 may spread from neuron to neuron over time
488 in worm. Although the six TRN soma are relatively distant from the two HSN soma (1/2-1/3 body
489 length or ~30-50 μm), PTL-1 is also enriched in TRN processes which pass nearby the HSNs
490 (Fig. 4A2). Two TRNs (the PLM pair) also form chemical synapses with the HSNs (White et al.,
491 1986). Future work could leverage synaptic transmission mutants to test whether this represents
492 a site of PTL-1 spread (Miller et al., 1996; McColluch et al., 2017). If the hypothetical PTL-1
493 spread is synaptic, genetically perturbing TRN neurotransmission may phenocopy our targeted
494 manipulations described above, suppressing HSN dysfunction. Moreover, we found that
495 fluorescently tagged PTL-1 did not interfere with PTL-1-dependent degeneration of the HSNs
496 (compare APOE4 strains with mNG tagged PTL-1 in Figs. 4,5 to non-tagged PTL-1 in Fig. 1G).
497 This raises the possibility of directly visualizing PTL-1 spread *in vivo*. With its simpler and fully
498 mapped nervous system, *C. elegans* offers a simple model to investigate how endogenous tau
499 propagates *in vivo* and contributes to APOE4-induced patterned neurodegeneration.
500 An alternate non-mutually exclusive hypothesis is that reduction of tau triggers
501 organism-wide or neuroprotective effects. The idea that tau levels set a susceptibility threshold
502 to many insults, not just tau-seeding pathology, may explain the broadly protective effects for
503 deleting tau in rodent models. For instance, Roberson et al. (2007) found that halving or deleting
504 endogenous tau rescued learning and memory as well as premature mortality in hAPP mice
505 without changing Aβ levels or plaques but also reduced susceptibility to chemically induced
506 seizures in otherwise wild-type backgrounds. Reducing tau also diminished spatial learning and

507 memory deficits after mild repetitive traumatic brain injury and attenuated axonopathy and other
508 histopathological changes in mice (Cheng et al, 2014). Systemic deletion of *ptl-1* reduces
509 lifespan in *C. elegans* (Chew et al., 2013; Chew et al., 2014) and was shown to be necessary
510 and sufficient in neurons for proper SKN-1-mediated response to environmental stressors
511 (Chew et al., 2015). It remains untested whether (and in what tissues) fine-tuning of PTL-1
512 levels may confer general protection against environmental and/or neurotoxic stressors in young
513 adult worms. Future studies should investigate this possibility.
514

515 **Materials and Methods**

516 **Strain Maintenance**

517 Unless otherwise noted, worms were maintained at room temperature (~20 °C) on NGM plates
518 seeded with OP50 bacteria as described (Brenner et al. 1974). Strains with extrachromosomal
519 transgenes were propagated using selectable fluorescent reporters. Strains are listed in order of
520 appearance in figures:

521 **Figures 1 and S2**

JPS1451 *vxEx1211[Pmyo-3::mCherry::UNC54UTR]*

RB809 *ptl-1(ok621) III*

JPS1453 *vxEx1213[Prab-3::ND18ApoE4::UNC54UTR + Pmyo-3::mCherry::UNC54UTR]*

JPS1455 *vxEx1215[Prab-3::ND18ApoE4::UNC54UTR + Pmyo-3::mCherry::UNC54UTR]; ptl-1(ok621) III*

Figure 2

JPS1451 *vxEx1211[Pmyo-3::mCherry::UNC54UTR]*

JPS1453 *vxEx1213[Prab-3::ND18ApoE4::UNC54UTR + Pmyo-3::mCherry::UNC54UTR]*

Figures 3, S5, and S6

JPS1666 *vxIs591[ptph-1::GFP::unc-54UTR]; vxEx1211[Pmyo-3::mCherry::UNC54UTR]*

JPS1664 *vxIs591[ptph-1::GFP::unc-54UTR]; vxEx1211[Pmyo-3::mCherry::UNC54UTR]; ptl-1(ok621) III*

JPS1667 *vxIs591[ptph-1::GFP::unc-54UTR]; vxEx1213[Prab-3::ND18ApoE4::UNC54UTR + Pmyo-3::mCherry::UNC54UTR]*

JPS1778 *vxIs591[ptph-1::GFP::unc-54UTR]; vxEx1213[Prab-3::ND18ApoE4::UNC54UTR + Pmyo-3::mCherry::UNC54UTR]; ptl-1(ok621) III*

JPS1779 *vxIs59[ptph-1::GFP::unc-54UTR]; vxEx1213[Prab-3::ND18ApoE4::UNC54UTR + Pmyo-3::mCherry::UNC54UTR]; ptl-1(ok621) III*

Figure 4

JPS1571 *vxIs591[ptph-1::GFP::unc-54UTR]*

JPS1828 *vxEx1511[Pmec-17::EGL-1::egl-1UTR]*; *ptl-1(pg73[PTL-1::mNeonGreen])*

TU253 *mec-4(u253) X*

JPS1500 *vxIs824[prab-3::ND18ApoE4::UNC54UTR, pmyo-2::mCherry::UNC54UTR]; ptl-1(pg73[PTL-1::mNeonGreen])*

JPS1839 vx*Is824[prab-3::ND18ApoE4::UNC54UTR, pmyo-2::mCherry::UNC54UTR]; ptl-1(pg73[PTL-1::mNeonGreen]); vxEx1511[Pmec-17::EGL-1::egl-1UTR]*

JPS1709 *vxIs824[prab-3::ND18ApoE4::UNC54UTR, pmyo-2::mCherry::UNC54UTR]; ptl-1(pg73[PTL-1::mNeonGreen]); mec-4(u253) X*

Figure 5

JPS1571 *vxIs591[ptph-1::GFP::unc-54UTR]*

GN655 *ptl-1(pg73[PTL-1::mNeonGreen])*

JPS1456 *ptl-1(pg73[PTL-1::mNeonGreen]); vxEx1216[Pmec-17::ptl-1 sense and antisense CDS + Punc-122::RFP]*

JPS1819 *ptl-1(syb8686 syb8597 pg73[LoxP::PTL-1::mNeonGreen::LoxP) III; hrtSi99[Pmec-17::Cre]*

JPS1872 *ptl-1(syb8686 syb8597 pg73) III; mirIs42[Pche-2::Cre + Plin-44::GFP]*

JPS1500 *vxIs824[prab-3::ND18ApoE4::UNC54UTR, pmyo-2::mCherry::UNC54UTR]; ptl-1(pg73[PTL-1::mNeonGreen])*

JPS1581 *vxIs824[prab-3::ND18ApoE4::UNC54UTR, pmyo-2::mCherry::UNC54UTR]; ptl-1(pg73[PTL-1::mNeonGreen]); vxEx1216[Pmec-17::ptl-1 sense and antisense CDS + Punc-122::RFP]*

JPS1582 *vxIs824[prab-3::ND18ApoE4::UNC54UTR, pmyo-2::mCherry::UNC54UTR]; ptl-1(pg73[PTL-1::mNeonGreen]); vxEx1216[Pmec-17::ptl-1 sense and antisense CDS + Punc-122::RFP]*

JPS1823 *vxIs824[prab-3::ND18ApoE4::UNC54UTR, pmyo-2::mCherry::UNC54UTR]; ptl-1(syb8686 syb8597 pg73[LoxP::PTL-1::mNeonGreen::LoxP) III; hrtSi99[Pmec-17::Cre]*

JPS1824 *vxIs824[prab-3::ND18ApoE4::UNC54UTR, pmyo-2::mCherry::UNC54UTR]; ptl-1(syb8686 syb8597 pg73[LoxP::PTL-1::mNeonGreen::LoxP) III; hrtSi99[Pmec-17::Cre]*

JPS1898 *vxEx1604[pRAB-3::mCherry::unc-54utr]*; *ptl-1(syb8686 syb8597 pg73[LoxP::PTL-1::mNeonGreen::LoxP) III; hrtSi99[Pmec-17::Cre]*

JPS1899 *vxEx1605[pRAB-3::mCherry::unc-54utr + Prab-3::ND18ApoE4::UNC54UTR]*; *ptl-1(syb8686 syb8597 pg73[LoxP::PTL-1::mNeonGreen::LoxP) III; hrtSi99[Pmec-17::Cre]*

JPS1897 *vxIs824[prab-3::ND18ApoE4::UNC54UTR, pmyo-2::mCherry::UNC54UTR];ptl-1(syb8686 syb8597 pg73) III; mirIs42[Pche-2::Cre + Plin-44::GFP]/+*

Figure S8

GN655 *ptl-1(pg73[PTL-1::mNeonGreen])*

JPS1500 *vxIs824[prab-3::ND18ApoE4::UNC54UTR, pmyo-2::mCherry::UNC54UTR]; ptl-1(pg73[PTL-1::mNeonGreen])*

JPS1828 *vxEx1511[Pmec-17::EGL-1::egl-1UTR]*; *ptl-1(pg73[PTL-1::mNeonGreen])*

JPS1456 *ptl-1(pg73[PTL-1::mNeonGreen]); vxEx1216[Pmec-17::ptl-1 sense and antisense CDS + Punc-122::RFP]*

JPS1819 *ptl-1(syb8686 syb8597 pg73[LoxP::PTL-1::mNeonGreen::LoxP) III; hrtSi99[Pmec-17::Cre]*

522 **Generation of strains**

523 Presence of the 1933 bp deletion in *ptl-1* allele *ok621* was confirmed by PCR using the following
524 primers (written in 5'-3' orientation):

Forward: CTGGAAATTTGTTGGGCAGT

Reverse: TGAACCGAAGCCTAAACCAG

525 We sought to independently confirm the effect of pan-neuronal APOE4 on egg laying as well as
526 to test other behaviors with new extrachromosomal transgenic strains that carry a new reporter
527 that minimized effects on multiple behaviors. We transformed wild-type N2 with 20 ng/μL of the
528 APOE4 plasmid pPS90 (Sae-Lee et al., 2020) along with 10 ng/μL of the pCFJ104 mCherry
529 body wall reporter (Frøkjaer-Jensen et al., 2008) to generate the new extrachromosomal strain
530 JPS1453. In parallel, we transformed the *ptl-1*(*ok621*) mutant strain RB809 with the same DNA
531 mixture yielding the APOE4;Δ*ptl-1* strain JPS1455. We also generated control strain JPS1451
532 that carries the mCherry reporter alone.

533 To visualize HSN axons, we first used the GFP reporter strain JPS1571. This strain was
534 crossed with JPS1451 and JPS1453 to yield the control and APOE4 strains JPS1666 and
535 JPS1667, respectively. JPS1666 was then crossed with RB809 to yield the *Ptph-1::gfp*;Δ*ptl-1*
536 strain JPS1664. JPS1667 was crossed with RB809 to yield APOE4;Δ*ptl-1*, from which two
537 independent isolates were obtained, JPS1778 and JPS1779, to partly control for genetic
538 background (Fig. 3). In our independent reporter lines, we transformed strain JPS1819 with 20
539 ng/uL of the mCherry reporter plasmid pGH8 without or with 40 ng/uL APOE4 plasmid pPS90 to
540 yield strains JPS1898 and JPS1899 (Fig. 5B3).

541 **Cell-specific gene knockdown**

542 To knock down *ptl-1* specifically in the touch receptor neurons (TRNs), we followed previous
543 methods by Esposito et al. (See Fig. 1 of Esposito et al., 2007). The *mec-17* promoter (1535 bp)
544 was fused with either sense or antisense of *ptl-1* coding region (820 bp) to generate separate
545 DNA fragments using the following primers (written in 5'-3' orientation):

A

Forward: GGCTTGAATAATCCCTATTATAGCC

Reverse: GAAATTACCTGAAATTTCGTGGGG

B

Forward: GAGAAAACGGCCAATTGACGC

Reverse: GGCTATAATAGGGATTATTCAAGCCGATCGAATCGTCTCACAACTG

C

Forward: GAGAAAACGGCCAATTGACGC

Reverse: CCCCACGAAATTTCAGGTAATTTCGATCGAATCGTCTCACAACTG

D

Forward: CGTCGCGCTAACAGTTCTAG

Reverse: CCAAAGGTTAACGCCAAATTTG

E

Forward: CGTCGCGCTAACAGTTCTAG

Reverse: CAAGTGAAAGCGTGGTCCGATC

546 Fragments D and E were mixed in equimolar amounts, along with a selectable RFP
547 coelomocyte marker (Addgene Plasmid #8938), to a final concentration of 80 ng/µL. This DNA
548 mix was transformed into the *ptl-1*::*mNeonGreen* strain GN655 (PTL-1::mNG; Krieg et al.,
549 2017). The resultant strain, JPS1456, expresses *ptl-1* dsRNA fragments in the TRNs. JPS1456
550 was crossed into JPS1500, which carries an integrated pan-neuronal APOE4 transgene; this
551 yielded APOE4;TRNs::*ptl-1* KD from which two independent isolates were obtained, JPS1581
552 and JPS1582, to partly control for genetic background.

553 **Cell-specific gene knockout**

554 To knock out *ptl-1* in the TRNs, we commissioned SUNY Biotech to generate the strain
555 PHX8686 which harbors *LoxP* sites flanking the *ptl-1* genetic locus in the strain GN655.
556 PHX8686 was crossed into MSB1167, a transgenic line in which Cre recombinase is expressed
557 under control of the *mec-17* promoter (Harterink et al., 2018). This yielded the TRNs::*ptl-1* KO
558 strain JPS1819. The presence of PTL-1::mNG in the TRNs was determined with epifluorescent
559 microscopy. Lastly, JPS1819 was crossed into JPS1500 to yield APOE4;TRNs::*ptl-1* KO, from

560 which two independent isolates were obtained, JPS1823 and JPS1824, to partly control for
561 genetic background.
562 Similarly, knockout of *ptl-1* in the *che-2*-expressing subset of sensory neurons (CHEs)
563 was achieved by crossing PHX8686 into FX16644, a transgenic line in which Cre recombinase
564 is expressed under control of the *che-2* promoter (National BioResource Project, Japan). This
565 yielded the CHEs::*ptl-1* KO strain JPS1872. However, subsequent crossing into JPS1500
566 resulted in synthetic lethality in animals homozygous for the CHEs-specific Cre transgene.
567 Thus, heterozygotes were selected for egg laying behavior assays.
568 **Cell-specific ablation**
569 To genetically ablate the TRNs, we used the TRN-specific *mec-17* promoter to express *egl-1* in
570 an extrachromosomal array in strain JPS1828 (Wu et al., 2025). This strain was crossed into
571 JPS1500, a strain carrying an integrated pan-neuronal APOE4 transgene and a *Punc-122*::*gfp*
572 reporter, to yield strain JPS1839. Additionally, we crossed JPS1500 into TU253, which carries a
573 *mec-4* loss-of-function mutation (O'Hagan et al., 2004), to yield the APOE4;*mec-4*(*lf*) strain
574 JPS1709.
575 **Sterilization**
576 To inspect HSN neuron health without confounding effects of the bagging phenotype, worms
577 were sterilized as previously described (Mitchell et al., 1979). In brief, seeded plates were
578 pretreated with 600 mL of 0.8 mM 5'-fluorodeoxyuridine (FUdR; FUdR plates). Mid- to late-stage
579 L4 stage worms were transferred onto FUDR plates and moved to fresh FUdR plates every 1-2
580 days as needed.
581 **Behavioral assays**
582 Behavioral assays were performed on either 60 mm (medium) or 35 mm (small) NGM plates,
583 seeded or not with OP50 bacteria as described per assay. All assays were performed at room
584 temperature (20° C) unless stated otherwise. Assays began with day 1 adults (D1), 24 hours
585 after initial incubation on FUDR plates (if applicable), until a significant difference between

586 control and APOE4 worms was observed. Completely immobile worms or those which escaped
587 from the side of the plate were omitted from assays and final quantifications.

588 **Gentle touch**

589 Methods adapted from Chalfie and Sulston (1981). In brief, 20-30 worms were moved to
590 medium NGM-OP50 plates. To test gentle touch sensitivity, an eyelash hair, affixed by its shaft
591 to a pipette tip, was used to deliver mechanical stimuli to worms. Gentle strokes were applied to
592 the posterior and anterior of the animal. Six paired anterior and posterior stimuli were applied,
593 with an interstimulus interval of approximately 1.5 seconds to avoid habituation. Gentle touch
594 sensitivity was quantified per worm as the fraction of responses to stimuli out of 12.

595 **Harsh touch**

596 Methods adapted from Li et al. (2011). In brief, 20-30 worms were moved to medium NGM-
597 OP50 plates. To test harsh gentle touch sensitivity, a single prod was delivered to the mid-body
598 using a platinum pick. Five technical replicates were performed per worm per strain. Harsh
599 touch sensitivity was quantified per replicate as the proportion of responsive worms.

600 **Pharyngeal pumping**

601 Methods adapted from Avery and Shtonda (2003). In brief, 30-40 worms were first moved to
602 medium NGM-OP50 plates. Worms were allowed to roam for at least 30 minutes. Individual
603 animals were then tracked for 20 seconds and pharyngeal bulb contractions were manually
604 tallied with a handheld click counter. Pumping rate was quantified per worm as pumps per
605 minute.

606 **Bagging**

607 Methods adapted from Sae-Lee et al. (2020). In brief, at least 30-40 L4-stage worms were
608 moved to medium NGM-OP50 plates. Worms were scored daily for the internal hatching or
609 “bagging” phenotype based on presence or absence of several late-stage eggs and/or hatched
610 larvae within the uterus; this is often accompanied by general lethargy plus distension of the
611 worm midbody as previously described (Trent et al., 1983). Bagging worms were tallied and
612 discarded while non-bagging worms were transferred to a fresh medium NGM-OP50 plate.

613 Worms were scored in this fashion from D1 to D4 of adulthood. Bagging incidence was
614 quantified per replicate as the cumulative percentage of bagging worms summed across D1-4
615 out of the original total.

616 **Long-term locomotion**

617 Methods adapted from Nordquist et al. (2018). Single worms were moved to the center of a
618 small NGM plate uniformly seeded with OP50 such that the lawn covered the entirety of the
619 NGM surface. Animals were incubated on these assay plates overnight at 22°C. Groups of at
620 least 8 worms per genotype were tested on two separate days as also described by Nordquist
621 et al. After 18 hours, the worms were removed from their plates and a transparent grid guide
622 was used to determine the number of ~5 mm^2 regions (32 in total) traversed on the assay plate.
623 Regions encompassing parts of the agar that split or pulled away from the plastic of the plate
624 were omitted from the total. Long-term locomotion was quantified per worm as the proportion of
625 traversed regions on the assay plate out of the total.

626 **Short-term locomotion**

627 Methods adapted from Topalidou et al. (2017). In brief, 8-10 worms were moved to the center of
628 a medium NGM-OP50 plate that was uniformly seeded such that the bacterial lawn extended
629 across the entire medium surface. After 10 minutes, worms were removed and their final
630 positions marked on the plate. Groups of least 15 worms per genotype were tested on two
631 separate days as previously described (Nordquist et al., 2018). Radially dispersed distance was
632 recorded. Short-term locomotion was quantified per worm as the distance (cm) from the center
633 to final positions.

634 **Swim-to-crawl gait transition**

635 Methods adapted from Vidal-Gadea et al. (2011). Before testing, 25-40 worms were moved to a
636 medium NGM plate and allowed to roam for ~15 minutes so excess OP50 could be removed.
637 Meanwhile, assay plates were prepared by first drawing a 0.5 cm radius border on the plastic
638 behind its center. Next, 10 uL of liquid NGM was pipetted to the very center of the assay plate
639 surface. Worms were then picked to the center of the puddle on the assay plate and a 15-

640 minute timer was started. As the puddle dried, swimming worms began to escape to the solid
641 surface, transition to a crawling gait, and disperse away from the puddle. Gait transition was
642 quantified per replicate as the proportion of worms that escaped and crawled past the 0.5 cm
643 border in under 15 minutes.

644 **Microscopy**

645 Epifluorescent microscopy was performed on an Olympus IX51 inverted microscope with an
646 Olympus UPlanFL N 40X/0.75 NA objective and X-Cite FIRE LED Illuminator (Excelitas
647 Technologies Corp.). Images were captured using a Retiga 2000R CCD camera (QImaging)
648 and QCapture Pro 6.0 software.

649 Worms were sterilized with FUDR as described above to prevent internally hatching
650 larvae that may affect HSN morphology. Worms were then mounted on 2% agarose pads and
651 immobilized using 50 mM sodium azide. All imaging per pad took place within 30 minutes of
652 mounting.

653 The same fluorescence intensity settings were used to image all HSN soma and
654 proximal axons via a GFP reporter. Importantly, imaging was restricted to worms that lay in a
655 strictly lateral orientation (i.e., on the right or left side with minimal twisting about the long axis of
656 the animal). This ensured both the soma and proximal axon of a given HSN neuron were in
657 approximately the same focal plane. We determined the orientation of mounted worms using the
658 fluorescent co-injection marker. This marker labels body wall and vulval musculature with
659 mCherry, visualizable in the red channel. In single focal planes, the labeled vulval muscles
660 either appear as an x-shape from a ventral viewpoint or a v-shape if the animal laid directly on
661 its right or left side as described above (See also Fig. 1 of Collins and Koelle, 2020).
662 Incidentally, the HSN GFP reporter also labels the VC4 and VC5 motor neurons which are
663 visible in the same focal plane. These guides helped restrict our microscopy to animals in the
664 desired orientation described above.

665 After imaging, morphometrics of HSN soma and proximal axons were calculated in
666 ImageJ (Schneider et al., 2012). Positions of HSN soma were determined by measuring the

667 lengths of the vector from the soma to the ventral nerve cord (HSN-VNC, met at a
668 perpendicular) and the vector to the vulval area in between VCs4,5 (HSN-vulva). These
669 measurements were also collapsed into a single metric as previously described (Asakura et al.,
670 2007). This metric, represented by θ, is the angle in degrees between the HSN-vulva
671 (hypotenuse) and HSN-VNC (adjacent) vectors (i.e., arccosine of their ratio).

672 HSN proximal axon lengths were calculated with the NeuronJ plugin for ImageJ using
673 default settings (Meijering et al., 2004). Traces were made by following the proximal axon from
674 anterior face of the HSN soma to the point at which the axon exits the focal plane ventrally in
675 the vulval area. Ectopic sprouts from the soma or proximal axon were excluded from tracing. In
676 the rare (<5% frequency) cases where ectopic sprouts were present on the proximal axon, the
677 shortest ventral- and vulval-directed course was traced for all strains imaged.

678 Full HSN axons were imaged in mid- to late-L4 stage worms when full projection to the
679 head region is typically complete (Garriga et al., 1993). Worms with very dim GFP fluorescence
680 were excluded from scoring, as it was ambiguous whether axons failed to project or the reporter
681 transgene was not yet highly enough expressed.

682 To capture images of PTL-1::mNG strains, an increased exposure time and intensity
683 setting were required compared to HSN GFP reporter strains. Because some TRN processes
684 span nearly the entire animal length, we chose to focus on soma to quantify PTL-1::mNG signal
685 in TRNs::*ptl-1* KD strain JPS1456 and control strain GN655 (See Fig. 4). Depending on animal
686 orientation, bilateral TRN soma were identifiable based on the naturally asymmetric positioning
687 of the AVM and PVM class neurons (Arnold et al., 2020). The VCs4,5 neurons were almost
688 always visualizable regardless of orientation, making them ideal for internal controls.
689 Fluorescence intensity was quantified in ImageJ in day 1 adults.

690 In the TRNs::*ptl-1* KO strain JPS1819, *LoxP*-flanked *ptl-1* is presumably excised by Cre
691 recombinase whose expression is driven by the *mec-17* promoter (Harterink et al., 2018).
692 Although *mec-17* expression begins embryonically in ALM and PLM class TRNs (Roux et al.,
693 2023), residual PTL-1::mNG is still present by at least L4 stage of development; PTL-1::mNG is

694 qualitatively fainter in those cells compared to like-aged control animals (GN655 strain). Thus,
695 selection for animals with lacking PTL-1::mNG in PLM neurons was conducted in at least day 1
696 adults to avoid ambiguity. This selection strategy was also employed in the TRNs::EGL-1 strain
697 JPS1828 to identify animals with genetically ablated TRNs.

698 **Western blotting**

699 Worms were washed twice with 5% sucrose and twice with 50 mM NaCl before being
700 flash frozen with 5µl glass beads. For worm lysis, 2% PMSF was added to 2x Laemmli buffer.
701 This buffer was then addedto the frozen samples to achieve a 1x concentration. Finally, 5% β-
702 mercaptoethanol (BME) was added to the samples, followed by bead beating for 30 seconds.
703 Samples were spun down through centrifugation for 2 minutes at 15,000 g. The samples were
704 then boiled a t 95℃ for 5 minutes. An additional 2-minute centrifugation was performed to clear
705 debris prior to measuring protein concentration with Qubit Protein Assay Kit (Thermo Scientific,
706 #Q33211).

707 20 µg of protein per sample was loaded on Invitrogen™ NuPAGE™ Bis-Tris Mini
708 Protein Gels (4–12%, 1.0–1.5 mm, Invitrogen, #NP0335) and separated at 80-120 V in
709 1X MES SDS running buffer. Proteins were transferred onto a PVDF membrane
710 (Thermo Scientific, #88518) at 30V for 1 hour.

711 Membranes were blocked in 1X TBS Tween 20 Buffer (Thermo Scientific, #28360)
712 containing 5% milk. Flag tag and actin were probed with primary antibodies: Monoclonal
713 ANTI-FLAG® M2 antibody produced in mouse (1:2,000, Sigma-Aldrich, #F3165) and
714 Anti-Actin Mouse Monoclonal Antibody [clone: C4] (1:500, MP Biomedicals,
715 #08691001), respectively. A secondary antibody, Goat anti-Mouse IgG (H+L)
716 Superclonal™ Secondary Antibody, Alexa Fluor™ 488 (1:4,000, Invitrogen, #A28175)
717 was used after flag and actin probing. Finally, an Amersham™ Typhoon™ RGB was
718 utilized for visualization.

719 **Statistical analysis**

720 All data are presented as the mean ± SEM. Plotted data points represent individuals or the
721 average across a single replicate as indicated in figures. Total sample size (N) is indicated in
722 figure legends. Behavioral assays and microscopy scoring were performed blind to genotype.
723 Planned χ^2 tests of independence were performed for statistical comparisons of gait transition
724 (escaped vs. not escaped), bagging (yes vs. no), and HSN axon scoring (normal vs. abnormal)
725 in Excel 2022 (365 MSO, Version 2510 Build 16.0.19328.20190, 64-bit). Touch, pumping, and
726 locomotion behaviors, HSN axon length, HSN soma position, and fluorescence intensity were
727 compared with planned, Student t-tests or post hoc comparisons following two-way ANOVA
728 tests (SPSS, v29.0.2.0, IBM).
729

730 **Acknowledgements**

731 We would like to thank Drs. Miriam B. Goodman and Michael Krieg for sharing strains GN655
732 and MSB1167, respectively, and SUNY Biotech for engineering PHX8686. Some strains were
733 also provided by the *Caenorhabditis* Genetics Center, which is funded by the NIH Center for
734 Research Resources. We also thank Chelsea Webber for constructive feedback on manuscript
735 drafts and Dr. Lotti Brose and Anna Krauss for preliminary experiments with APOE4; Δ*ptl-1*
736 animals.

737

738 **Footnotes**

739 **Author contributions**

740 Conceptualization: J.T.P., E.A.C.; Methodology: E.A.C., Z.W., J.T.P.; Investigation: E.A.C.,
741 Z.W., B.M.B., C.J.W., E.S.-C., J.T.P.; Writing – original draft: E.A.C., J.T.P.; Writing – review
742 and editing: E.A.C., Z.W., C.J.W., E.S.-C., J.T.P.; Funding acquisition: E.S.-C., J.T.P.

743 **Funding**

744 This work was funded in part by the NIH (R01GM122463, RF1AG057355, R21OD032463 -
745 J.T.P.) Waggoner Fellowship for Alcohol Research (J.T.P.), David and Ellen Berman
746 Fellowships for Huntington's Research (J.T.P.), George and Karen Casey (J.T.P.), Pine Family
747 Foundation (J.T.P.), CNS Catalyst Grant (J.T.P. and E.S.C.), National Institutes of Health (NIH)
748 NIGMS (R35GM138340) (E.S.C.), NIH T32 MH106454 (C.J.W.), Welch Foundation (F-2133-
749 20230405) (E.S.C.), and F.M. Jones and H.L. Bruce Graduate Fellowship (Z.W.).

750 **Data availability**

751 All relevant data can be found either within the article or in its supplementary information
752 section. Raw data is available upon request.

753 **Competing interests**

754 The authors declare no competing or financial interests.

755

756

757 **References**

758 1. Andrews-Zwilling, Y., Bien-Ly, N., Xu, Q., Li, G., Bernardo, A., Yoon, S. Y., Zwilling, D., Yan,
759 T. X., Chen, L., and Huang, Y. (2010). Apolipoprotein E4 causes age- and Tau-dependent
760 impairment of GABAergic interneurons, leading to learning and memory deficits in mice. *The*
761 *Journal of neuroscience : the official journal of the Society for Neuroscience*, *30*(41), 13707–
762 13717. https://doi.org/10.1523/JNEUROSCI.4040-10.2010
763 2. Aquino Nunez, W., Combs, B., Gamblin, T. C., and Ackley, B. D. (2022). Age-dependent
764 accumulation of tau aggregation in *Caenorhabditis elegans*. *Frontiers in aging*, *3*, 928574.
765 https://doi.org/10.3389/fragi.2022.928574
766 3. Arnold, M. L., Cooper, J., Grant, B. D., & Driscoll, M. (2020). Quantitative Approaches for
767 Scoring in vivo Neuronal Aggregate and Organelle Extrusion in Large Exopher Vesicles in
768 C. elegans. *Journal of visualized experiments : JoVE*, (163), 10.3791/61368.
769 https://doi.org/10.3791/61368
770 4. Asakura, T., Ogura, K., and Goshima, Y. (2007). UNC-6 expression by the vulval precursor
771 cells of Caenorhabditis elegans is required for the complex axon guidance of the HSN
772 neurons. *Developmental biology*, *304*(2), 800–810.
773 https://doi.org/10.1016/j.ydbio.2007.01.028
774 5. Avery, L., and Shtonda, B. B. (2003). Food transport in the C. elegans pharynx. *The Journal*
775 *of experimental biology*, *206*(Pt 14), 2441–2457. https://doi.org/10.1242/jeb.00433
776 6. Avery, L., and You, Y. J. (2012). C. elegans feeding. *WormBook : the online review of C.*
777 *elegans biology*, 1–23. https://doi.org/10.1895/wormbook.1.150.1
778 7. Baskoylu, S. N., Yersak, J., O'Hern, P., Grosser, S., Simon, J., Kim, S., Schuch, K.,
779 Dimitriadi, M., Yanagi, K. S., Lins, J., and Hart, A. C. (2018). Single copy/knock-in models of
780 ALS SOD1 in C. elegans suggest loss and gain of function have different contributions to
781 cholinergic and glutamatergic neurodegeneration. *PLoS genetics*, *14*(10), e1007682.
782 https://doi.org/10.1371/journal.pgen.1007682
783 8. Benbow, S. J., Strovas, T. J., Darvas, M., Saxton, A., and Kraemer, B. C. (2020). Synergistic
784 toxicity between tau and amyloid drives neuronal dysfunction and neurodegeneration in
785 transgenic C. elegans. *Human molecular genetics*, *29*(3), 495–505.
786 https://doi.org/10.1093/hmg/ddz319
787 9. Benzing, W. C., and Mufson, E. J. (1995). Apolipoprotein E immunoreactivity within
788 neurofibrillary tangles: relationship to Tau and PHF in Alzheimer's disease. *Experimental*
789 *neurology*, *132*(2), 162–171. https://doi.org/10.1016/0014-4886(95)90021-7
790 10. Bookheimer, S. Y., Strojwas, M. H., Cohen, M. S., Saunders, A. M., Pericak-Vance, M. A.,
791 Mazziotta, J. C., and Small, G. W. (2000). Patterns of brain activation in people at risk for
792 Alzheimer's disease. *The New England journal of medicine*, *343*(7), 450–456.
793 https://doi.org/10.1056/NEJM200008173430701

794 11. Braak, H., and Braak, E. (1991). Neuropathological stageing of Alzheimer-related changes.
795 *Acta neuropathologica*, *82*(4), 239–259. https://doi.org/10.1007/BF00308809
796 12. Braak, H., & Del Tredici, K. (2011). Alzheimer's pathogenesis: is there neuron-to-neuron
797 propagation?. *Acta neuropathologica*, *121*(5), 589–595. https://doi.org/10.1007/s00401-011-
798 0825-z
799 13. Brenner S. (1974). The genetics of Caenorhabditis elegans. *Genetics*, *77*(1), 71–94.
800 https://doi.org/10.1093/genetics/77.1.71
801 14. Brecht, W. J., Harris, F. M., Chang, S., Tesseur, I., Yu, G. Q., Xu, Q., Dee Fish, J., Wyss-
802 Coray, T., Buttini, M., Mucke, L., Mahley, R. W., and Huang, Y. (2004). Neuron-specific
803 apolipoprotein e4 proteolysis is associated with increased tau phosphorylation in brains of
804 transgenic mice. *The Journal of neuroscience : the official journal of the Society for*
805 *Neuroscience*, *24*(10), 2527–2534. https://doi.org/10.1523/JNEUROSCI.4315-03.2004
806 15. Butner, K. A., and Kirschner, M. W. (1991). Tau protein binds to microtubules through a
807 flexible array of distributed weak sites. *The Journal of cell biology*, *115*(3), 717–730.
808 https://doi.org/10.1083/jcb.115.3.717
809 16. Chalfie, M., and Sulston, J. (1981). Developmental genetics of the mechanosensory
810 neurons of Caenorhabditis elegans. *Developmental biology*, *82*(2), 358–370.
811 https://doi.org/10.1016/0012-1606(81)90459-0
812 17. Chalfie, M., and Thomson, J. N. (1979). Organization of neuronal microtubules in the
813 nematode Caenorhabditis elegans. *The Journal of cell biology*, *82*(1), 278–289.
814 https://doi.org/10.1083/jcb.82.1.278
815 18. Chalfie, M., and Thomson, J. N. (1982). Structural and functional diversity in the neuronal
816 microtubules of Caenorhabditis elegans. *The Journal of cell biology*, *93*(1), 15–23.
817 https://doi.org/10.1083/jcb.93.1.15
818 19. Chalfie, M., Sulston, J. E., White, J. G., Southgate, E., Thomson, J. N., and Brenner, S.
819 (1985). The neural circuit for touch sensitivity in Caenorhabditis elegans. *The Journal of*
820 *neuroscience : the official journal of the Society for Neuroscience*, *5*(4), 956–964.
821 https://doi.org/10.1523/JNEUROSCI.05-04-00956.1985
822 20. Chang, A. J., Chronis, N., Karow, D. S., Marletta, M. A., and Bargmann, C. I. (2006). A
823 distributed chemosensory circuit for oxygen preference in C. elegans. *PLoS biology*, *4*(9),
824 e274. https://doi.org/10.1371/journal.pbio.0040274
825 21. Clavaguera, F., Bolmont, T., Crowther, R. A., Abramowski, D., Frank, S., Probst, A., Fraser,
826 G., Stalder, A. K., Beibel, M., Staufenbiel, M., Jucker, M., Goedert, M., and Tolnay, M.
827 (2009). Transmission and spreading of tauopathy in transgenic mouse brain. *Nature cell*
828 *biology*, *11*(7), 909–913. https://doi.org/10.1038/ncb1901

829 22. Coakley, S., Ritchie, F. K., Galbraith, K. M., and Hilliard, M. A. (2020). Epidermal control of
830 axonal attachment via β-spectrin and the GTPase-activating protein TBC-10 prevents
831 axonal degeneration. *Nature communications*, *11*(1), 133. https://doi.org/10.1038/s41467-
832 019-13795-x
833 23. Cornblath, E. J., Li, H. L., Changolkar, L., Zhang, B., Brown, H. J., Gathagan, R. J., Olufemi,
834 M. F., Trojanowski, J. Q., Bassett, D. S., Lee, V. M. Y., and Henderson, M. X. (2021).
835 Computational modeling of tau pathology spread reveals patterns of regional vulnerability
836 and the impact of a genetic risk factor. *Science advances*, *7*(24), eabg6677.
837 https://doi.org/10.1126/sciadv.abg6677
838 24. Crespo-Biel, N., Theunis, C., Borghgraef, P., Lechat, B., Devijver, H., Maurin, H., and Van
839 Leuven, F. (2014). Phosphorylation of protein Tau by GSK3β prolongs survival of bigenic
840 Tau.P301L×GSK3β mice by delaying brainstem tauopathy. *Neurobiology of disease*, *67*,
841 119–132. https://doi.org/10.1016/j.nbd.2014.03.016
842 25. Daigle, I., and Li, C. (1993). apl-1, a Caenorhabditis elegans gene encoding a protein
843 related to the human beta-amyloid protein precursor. *Proceedings of the National Academy*
844 *of Sciences of the United States of America*, *90*(24), 12045–12049.
845 https://doi.org/10.1073/pnas.90.24.12045
846 26. Davis, A. A., Inman, C. E., Wargel, Z. M., Dube, U., Freeberg, B. M., Galluppi, A., Haines, J.
847 N., Dhavale, D. D., Miller, R., Choudhury, F. A., Sullivan, P. M., Cruchaga, C., Perlmutter, J.
848 S., Ulrich, J. D., Benitez, B. A., Kotzbauer, P. T., and Holtzman, D. M. (2020). *APOE*
849 genotype regulates pathology and disease progression in synucleinopathy. *Science*
850 *translational medicine*, *12*(529), eaay3069. https://doi.org/10.1126/scitranslmed.aay3069
851 27. de Calignon, A., Polydoro, M., Suárez-Calvet, M., William, C., Adamowicz, D. H., Kopeikina,
852 K. J., Pitstick, R., Sahara, N., Ashe, K. H., Carlson, G. A., Spires-Jones, T. L., and Hyman,
853 B. T. (2012). Propagation of tau pathology in a model of early Alzheimer's disease. *Neuron*,
854 *73*(4), 685–697. https://doi.org/10.1016/j.neuron.2011.11.033
855 28. DeVos, S. L., Miller, R. L., Schoch, K. M., Holmes, B. B., Kebodeaux, C. S., Wegener, A. J.,
856 Chen, G., Shen, T., Tran, H., Nichols, B., Zanardi, T. A., Kordasiewicz, H. B., Swayze, E. E.,
857 Bennett, C. F., Diamond, M. I., and Miller, T. M. (2017). Tau reduction prevents neuronal
858 loss and reverses pathological tau deposition and seeding in mice with tauopathy. *Science*
859 *translational medicine*, *9*(374), eaag0481. https://doi.org/10.1126/scitranslmed.aag0481
860 29. Eichel, K., Uenaka, T., Belapurkar, V., Lu, R., Cheng, S., Pak, J. S., Taylor, C. A., Südhof, T.
861 C., Malenka, R., Wernig, M., Özkan, E., Perrais, D., and Shen, K. (2022). Endocytosis in the
862 axon initial segment maintains neuronal polarity. *Nature*, *609*(7925), 128–135.
863 https://doi.org/10.1038/s41586-022-05074-5

30. Esposito, G., Di Schiavi, E., Bergamasco, C., and Bazzicalupo, P. (2007). Efficient and cell specific knock-down of gene function in targeted C. elegans neurons. *Gene*, *395*(1-2), 170–176. https://doi.org/10.1016/j.gene.2007.03.002
31. Faber, P. W., Alter, J. R., MacDonald, M. E., and Hart, A. C. (1999). Polyglutamine-mediated dysfunction and apoptotic death of a Caenorhabditis elegans sensory neuron. *Proceedings of the National Academy of Sciences of the United States of America*, *96*(1), 179–184. https://doi.org/10.1073/pnas.96.1.179
32. Fatouros, C., Pir, G. J., Biernat, J., Koushika, S. P., Mandelkow, E., Mandelkow, E. M., Schmidt, E., and Baumeister, R. (2012). Inhibition of tau aggregation in a novel Caenorhabditis elegans model of tauopathy mitigates proteotoxicity. *Human molecular genetics*, *21*(16), 3587–3603. https://doi.org/10.1093/hmg/dds190
33. Fiford, C. M., Ridgway, G. R., Cash, D. M., Modat, M., Nicholas, J., Manning, E. N., Malone, I. B., Biessels, G. J., Ourselin, S., Carmichael, O. T., Cardoso, M. J., Barnes, J., and Alzheimer's Disease Neuroimaging Initiative (2018). Patterns of progressive atrophy vary with age in Alzheimer's disease patients. *Neurobiology of aging*, *63*, 22–32. https://doi.org/10.1016/j.neurobiolaging.2017.11.002
34. Flavell, S. W., Raizen, D. M., and You, Y. J. (2020). Behavioral States. *Genetics*, *216*(2), 315–332. https://doi.org/10.1534/genetics.120.303539
35. Fortea, J., Pegueroles, J., Alcolea, D., Belbin, O., Dols-Icardo, O., Vaqué-Alcázar, L., Videla, L., Gispert, J. D., Suárez-Calvet, M., Johnson, S. C., Sperling, R., Bejanin, A., Lleó, A., and Montal, V. (2024). APOE4 homozygozity represents a distinct genetic form of Alzheimer's disease. *Nature medicine*, *30*(5), 1284–1291. https://doi.org/10.1038/s41591-024-02931-w
36. Friedhoff, P., Schneider, A., Mandelkow, E. M., and Mandelkow, E. (1998). Rapid assembly of Alzheimer-like paired helical filaments from microtubule-associated protein tau monitored by fluorescence in solution. *Biochemistry*, *37*(28), 10223–10230. https://doi.org/10.1021/bi980537d
37. Friedhoff, P., von Bergen, M., Mandelkow, E. M., Davies, P., and Mandelkow, E. (1998). A nucleated assembly mechanism of Alzheimer paired helical filaments. *Proceedings of the National Academy of Sciences of the United States of America*, *95*(26), 15712–15717. https://doi.org/10.1073/pnas.95.26.15712
38. Frøkjaer-Jensen, C., Davis, M. W., Hopkins, C. E., Newman, B. J., Thummel, J. M., Olesen, S. P., Grunnet, M., and Jorgensen, E. M. (2008). Single-copy insertion of transgenes in Caenorhabditis elegans. *Nature genetics*, *40*(11), 1375–1383. https://doi.org/10.1038/ng.248
39. Frost, B., and Diamond, M. I. (2010). Prion-like mechanisms in neurodegenerative diseases. *Nature reviews. Neuroscience*, *11*(3), 155–159. https://doi.org/10.1038/nrn2786

900 40. Fu, H., Hussaini, S. A., Wegmann, S., Profaci, C., Daniels, J. D., Herman, M., Emrani, S.,
901 Figueroa, H. Y., Hyman, B. T., Davies, P., and Duff, K. E. (2016). 3D Visualization of the
902 Temporal and Spatial Spread of Tau Pathology Reveals Extensive Sites of Tau
903 Accumulation Associated with Neuronal Loss and Recognition Memory Deficit in Aged Tau
904 Transgenic Mice. *PloS one*, *11*(7), e0159463. https://doi.org/10.1371/journal.pone.0159463
905 41. Fujiwara M, Ishihara T, Katsura I. (1999). A novel WD40 protein, CHE-2, acts cell-
906 autonomously in the formation of *C. elegans* sensory cilia. *Development*. 126(21):4839-48.
907 https://doi: 10.1242/dev.126.21.4839.
908 42. Gao, S., Guan, S. A., Fouad, A. D., Meng, J., Kawano, T., Huang, Y. C., Li, Y., Alcaire, S.,
909 Hung, W., Lu, Y., Qi, Y. B., Jin, Y., Alkema, M., Fang-Yen, C., and Zhen, M. (2018).
910 Excitatory motor neurons are local oscillators for backward locomotion. *eLife*, *7*, e29915.
911 https://doi.org/10.7554/eLife.29915
912 43. Garriga, G., Desai, C., and Horvitz, H. R. (1993). Cell interactions control the direction of
913 outgrowth, branching and fasciculation of the HSN axons of Caenorhabditis elegans.
914 *Development (Cambridge, England)*, *117*(3), 1071–1087.
915 https://doi.org/10.1242/dev.117.3.1071
916 44. Ghoshal, N., García-Sierra, F., Wuu, J., Leurgans, S., Bennett, D. A., Berry, R. W., and
917 Binder, L. I. (2002). Tau conformational changes correspond to impairments of episodic
918 memory in mild cognitive impairment and Alzheimer's disease. *Experimental neurology*,
919 *177*(2), 475–493. https://doi.org/10.1006/exnr.2002.8014
920 45. Goedert, M., Baur, C. P., Ahringer, J., Jakes, R., Hasegawa, M., Spillantini, M. G., Smith, M.
921 J., and Hill, F. (1996). PTL-1, a microtubule-associated protein with tau-like repeats from the
922 nematode Caenorhabditis elegans. *Journal of cell science*, *109 (Pt 11)*, 2661–2672.
923 https://doi.org/10.1242/jcs.109.11.2661
924 46. Gordon, P., Hingula, L., Krasny, M. L., Swienckowski, J. L., Pokrywka, N. J., and Raley-
925 Susman, K. M. (2008). The invertebrate microtubule-associated protein PTL-1 functions in
926 mechanosensation and development in Caenorhabditis elegans. *Development genes and*
927 *evolution*, *218*(10), 541–551. https://doi.org/10.1007/s00427-008-0250-z
928 47. Grundke-Iqbal, I., Iqbal, K., Quinlan, M., Tung, Y. C., Zaidi, M. S., and Wisniewski, H. M.
929 (1986). Microtubule-associated protein tau. A component of Alzheimer paired helical
930 filaments. *The Journal of biological chemistry*, *261*(13), 6084–6089.
931 48. Harterink, M., Edwards, S. L., de Haan, B., Yau, K. W., van den Heuvel, S., Kapitein, L. C.,
932 Miller, K. G., and Hoogenraad, C. C. (2018). Local microtubule organization promotes cargo
933 transport in *C. elegans* dendrites. *Journal of cell science*, *131*(20), jcs223107.
934 https://doi.org/10.1242/jcs.223107

935 49. Hashi, Y., Kotani, S., and Adachi, T. (2016). A nematode microtubule-associated protein,
936 PTL-1, closely resembles its mammalian counterparts in overall molecular architecture.
937 *Bioscience, Biotechnology, and Biochemistry*, *80*(6), 1107–1113.
938 https://doi.org/10.1080/09168451.2016.1141038
939 50. Horvitz H. R. (2003). Worms, life, and death (Nobel lecture). *Chembiochem : a European*
940 *journal of chemical biology*, *4*(8), 697–711. https://doi.org/10.1002/cbic.200300614
941 51. Huang, Y., Liu, X. Q., Wyss-Coray, T., Brecht, W. J., Sanan, D. A., and Mahley, R. W.
942 (2001). Apolipoprotein E fragments present in Alzheimer's disease brains induce
943 neurofibrillary tangle-like intracellular inclusions in neurons. *Proceedings of the National*
944 *Academy of Sciences of the United States of America*, *98*(15), 8838–8843.
945 https://doi.org/10.1073/pnas.151254698
946 52. Iba, M., Guo, J. L., McBride, J. D., Zhang, B., Trojanowski, J. Q., and Lee, V. M. (2013).
947 Synthetic tau fibrils mediate transmission of neurofibrillary tangles in a transgenic mouse
948 model of Alzheimer's-like tauopathy. *The Journal of neuroscience : the official journal of the*
949 *Society for Neuroscience*, *33*(3), 1024–1037. https://doi.org/10.1523/JNEUROSCI.2642-
950 12.2013
951 53. Izquierdo, E. J., and Beer, R. D. (2018). From head to tail: a neuromechanical model of
952 forward locomotion in *Caenorhabditis elegans*. *Philosophical transactions of the Royal*
953 *Society of London. Series B, Biological sciences*, *373*(1758), 20170374.
954 https://doi.org/10.1098/rstb.2017.0374
955 54. Jeganathan, S., Hascher, A., Chinnathambi, S., Biernat, J., Mandelkow, E. M., and
956 Mandelkow, E. (2008). Proline-directed pseudo-phosphorylation at AT8 and PHF1 epitopes
957 induces a compaction of the paperclip folding of Tau and generates a pathological (MC-1)
958 conformation. *The Journal of biological chemistry*, *283*(46), 32066–32076.
959 https://doi.org/10.1074/jbc.M805300200
960 55. Jeganathan, S., von Bergen, M., Brutlach, H., Steinhoff, H. J., and Mandelkow, E. (2006).
961 Global hairpin folding of tau in solution. *Biochemistry*, *45*(7), 2283–2293.
962 https://doi.org/10.1021/bi0521543
963 56. Jiang, W. I., Cao, Y., Xue, Y., Ji, Y., Winer, B. Y., Chandra, R., Zhang, X. F., Zhang, M.,
964 Singhal, N. S., Pierce, J. T., Chen, S., and Ma, D. K. (2025). Suppressing APOE4-induced
965 neural pathologies by targeting the VHL-HIF axis. *Proceedings of the National Academy of*
966 *Sciences of the United States of America*, *122*(5), e2417515122.
967 https://doi.org/10.1073/pnas.2417515122
968 57. Kfoury, N., Holmes, B. B., Jiang, H., Holtzman, D. M., and Diamond, M. I. (2012). Trans-
969 cellular propagation of Tau aggregation by fibrillar species. *The Journal of biological*
970 *chemistry*, *287*(23), 19440–19451. https://doi.org/10.1074/jbc.M112.346072

971 58. Köpke, E., Tung, Y. C., Shaikh, S., Alonso, A. C., Iqbal, K., and Grundke-Iqbal, I. (1993).
972 Microtubule-associated protein tau. Abnormal phosphorylation of a non-paired helical
973 filament pool in Alzheimer disease. *The Journal of biological chemistry*, *268*(32), 24374–
974 24384.
975 59. Koriath, C., Lashley, T., Taylor, W., Druyeh, R., Dimitriadis, A., Denning, N., Williams, J.,
976 Warren, J. D., Fox, N. C., Schott, J. M., Rowe, J. B., Collinge, J., Rohrer, J. D., and Mead,
977 S. (2019). ApoE4 lowers age at onset in patients with frontotemporal dementia and
978 tauopathy independent of amyloid-β copathology. *Alzheimer's and dementia (Amsterdam,*
979 *Netherlands)*, *11*, 277–280. https://doi.org/10.1016/j.dadm.2019.01.010
980 60. Kosik, K. S., Orecchio, L. D., Binder, L., Trojanowski, J. Q., Lee, V. M., and Lee, G. (1988).
981 Epitopes that span the tau molecule are shared with paired helical filaments. *Neuron*, *1*(9),
982 817–825. https://doi.org/10.1016/0896-6273(88)90129-8
983 61. Koutsodendris, N., Blumenfeld, J., Agrawal, A., Traglia, M., Grone, B., Zilberter, M., Yip, O.,
984 Rao, A., Nelson, M. R., Hao, Y., Thomas, R., Yoon, S. Y., Arriola, P., and Huang, Y. (2023).
985 Neuronal APOE4 removal protects against tau-mediated gliosis, neurodegeneration and
986 myelin deficits. *Nature aging*, *3*(3), 275–296. https://doi.org/10.1038/s43587-023-00368-3
987 62. Kowall, N. W., and Kosik, K. S. (1987). Axonal disruption and aberrant localization of tau
988 protein characterize the neuropil pathology of Alzheimer's disease. *Annals of neurology*,
989 *22*(5), 639–643. https://doi.org/10.1002/ana.410220514
990 63. Kraemer, B. C., Zhang, B., Leverenz, J. B., Thomas, J. H., Trojanowski, J. Q., and
991 Schellenberg, G. D. (2003). Neurodegeneration and defective neurotransmission in a
992 Caenorhabditis elegans model of tauopathy. *Proceedings of the National Academy of*
993 *Sciences of the United States of America*, *100*(17), 9980–9985.
994 https://doi.org/10.1073/pnas.1533448100
995 64. Krieg, M., Stühmer, J., Cueva, J. G., Fetter, R., Spilker, K., Cremers, D., Shen, K., Dunn, A.
996 R., and Goodman, M. B. (2017). Genetic defects in β-spectrin and tau sensitize *C. elegans*
997 axons to movement-induced damage via torque-tension coupling. *eLife*, *6*, e20172.
998 https://doi.org/10.7554/eLife.20172
999 65. Larsen, F. K., Baksh, R. A., McGlinchey, E., Langballe, E. M., Benejam, B., Beresford-
1000 Webb, J., McCarron, M., Coppus, A., Falquero, S., Fortea, J., Levin, J., Loosli, S. V., Mark,
1001 R., Rebillat, A. S., Zaman, S., and Strydom, A. (2024). Age of Alzheimer's disease diagnosis
1002 in people with Down syndrome and associated factors: Results from the Horizon 21
1003 European Down syndrome consortium. *Alzheimer's and dementia : the journal of the*
1004 *Alzheimer's Association*, *20*(5), 3270–3280. https://doi.org/10.1002/alz.13779
1005 66. Lee, S., Viqar, F., Zimmerman, M. E., Narkhede, A., Tosto, G., Benzinger, T. L., Marcus, D.
1006 S., Fagan, A. M., Goate, A., Fox, N. C., Cairns, N. J., Holtzman, D. M., Buckles, V., Ghetti,

1007 B., McDade, E., Martins, R. N., Saykin, A. J., Masters, C. L., Ringman, J. M., Ryan, N. S., …
1008 Dominantly Inherited Alzheimer Network (2016). White matter hyperintensities are a core
1009 feature of Alzheimer's disease: Evidence from the dominantly inherited Alzheimer network.
1010 *Annals of neurology*, *79*(6), 929–939. https://doi.org/10.1002/ana.24647
1011 67. Lee, V. M., and Trojanowski, J. Q. (1992). The disordered neuronal cytoskeleton in
1012 Alzheimer's disease. *Current opinion in neurobiology*, *2*(5), 653–656.
1013 https://doi.org/10.1016/0959-4388(92)90034-i
1014 68. Leroy, K., Yilmaz, Z., and Brion, J. P. (2007). Increased level of active GSK-3beta in
1015 Alzheimer's disease and accumulation in argyrophilic grains and in neurones at different
1016 stages of neurofibrillary degeneration. *Neuropathology and applied neurobiology*, *33*(1), 43–
1017 55. https://doi.org/10.1111/j.1365-2990.2006.00795.x
1018 69. Li, W., Kang, L., Piggott, B. J., Feng, Z., and Xu, X. Z. (2011). The neural circuits and
1019 sensory channels mediating harsh touch sensation in Caenorhabditis elegans. *Nature*
1020 *communications*, *2*, 315. https://doi.org/10.1038/ncomms1308
1021 70. Lima-Silva, T. B., Bahia, V. S., Carvalho, V. A., Guimarães, H. C., Caramelli, P., Balthazar,
1022 M., Damasceno, B., Bottino, C. M. C., Brucki, S. M. D., Nitrini, R., and Yassuda, M. S.
1023 (2013). Functional profile of patients with behavioral variant frontotemporal dementia
1024 (bvFTD) compared to patients with Alzheimer's disease and normal controls. *Dementia and*
1025 *neuropsychologia*, *7*(1), 96–103. https://doi.org/10.1590/S1980-57642013DN70100015
1026 71. Lin, L. C., Nana, A. L., Hepker, M., Hwang, J. L., Gaus, S. E., Spina, S., Cosme, C. G., Gan,
1027 L., Grinberg, L. T., Geschwind, D. H., Coppola, G., Rosen, H. J., Miller, B. L., and Seeley,
1028 W. W. (2019). Preferential tau aggregation in von Economo neurons and fork cells in
1029 frontotemporal lobar degeneration with specific MAPT variants. *Acta neuropathologica*
1030 *communications*, *7*(1), 159. https://doi.org/10.1186/s40478-019-0809-0
1031 72. Liu, L., Drouet, V., Wu, J. W., Witter, M. P., Small, S. A., Clelland, C., and Duff, K. (2012).
1032 Trans-synaptic spread of tau pathology in vivo. *PloS one*, *7*(2), e31302.
1033 https://doi.org/10.1371/journal.pone.0031302
1034 73. McCulloch, K. A., Qi, Y. B., Takayanagi-Kiya, S., Jin, Y., and Cherra, S. J., 3rd (2017). Novel
1035 Mutations in Synaptic Transmission Genes Suppress Neuronal Hyperexcitation in
1036 *Caenorhabditis elegans*. *G3 (Bethesda, Md.)*, *7*(7), 2055–2063.
1037 https://doi.org/10.1534/g3.117.042598
1038 74. McDermott, J. B., Aamodt, S., and Aamodt, E. (1996). ptl-1, a Caenorhabditis elegans gene
1039 whose products are homologous to the tau microtubule-associated proteins. *Biochemistry*,
1040 *35*(29), 9415–9423. https://doi.org/10.1021/bi952646n
1041 75. Meijering, E., Jacob, M., Sarria, J. C., Steiner, P., Hirling, H., and Unser, M. (2004). Design
1042 and validation of a tool for neurite tracing and analysis in fluorescence microscopy images.

1043 *Cytometry. Part A : the journal of the International Society for Analytical Cytology*, *58*(2),
1044 167–176. https://doi.org/10.1002/cyto.a.20022
1045 76. Meisl, G., Hidari, E., Allinson, K., Rittman, T., DeVos, S. L., Sanchez, J. S., Xu, C. K., Duff,
1046 K. E., Johnson, K. A., Rowe, J. B., Hyman, B. T., Knowles, T. P. J., and Klenerman, D.
1047 (2021). In vivo rate-determining steps of tau seed accumulation in Alzheimer's disease.
1048 *Science advances*, *7*(44), eabh1448. https://doi.org/10.1126/sciadv.abh1448
1049 77. Miller, K. G., Alfonso, A., Nguyen, M., Crowell, J. A., Johnson, C. D., and Rand, J. B. (1996).
1050 A genetic selection for Caenorhabditis elegans synaptic transmission mutants. *Proceedings*
1051 *of the National Academy of Sciences of the United States of America*, *93*(22), 12593–12598.
1052 https://doi.org/10.1073/pnas.93.22.12593
1053 78. Mitchell, D. H., Stiles, J. W., Santelli, J., and Sanadi, D. R. (1979). Synchronous growth and
1054 aging of Caenorhabditis elegans in the presence of fluorodeoxyuridine. *Journal of*
1055 *gerontology*, *34*(1), 28–36. https://doi.org/10.1093/geronj/34.1.28
1056 79. Mizumoto, K., and Shen, K. (2013). Interaxonal interaction defines tiled presynaptic
1057 innervation in C. elegans. *Neuron*, *77*(4), 655–666.
1058 https://doi.org/10.1016/j.neuron.2012.12.031
1059 80. Mocanu, M. M., Nissen, A., Eckermann, K., Khlistunova, I., Biernat, J., Drexler, D., Petrova,
1060 O., Schönig, K., Bujard, H., Mandelkow, E., Zhou, L., Rune, G., and Mandelkow, E. M.
1061 (2008). The potential for beta-structure in the repeat domain of tau protein determines
1062 aggregation, synaptic decay, neuronal loss, and coassembly with endogenous Tau in
1063 inducible mouse models of tauopathy. *The Journal of neuroscience : the official journal of*
1064 *the Society for Neuroscience*, *28*(3), 737–748. https://doi.org/10.1523/JNEUROSCI.2824-
1065 07.2008
1066 81. Natale, C., Barzago, M. M., and Diomede, L. (2020). *Caenorhabditis elegans* Models to
1067 Investigate the Mechanisms Underlying Tau Toxicity in Tauopathies. *Brain sciences*, *10*(11),
1068 838. https://doi.org/10.3390/brainsci10110838
1069 82. Nikoletopoulou, V., and Tavernarakis, N. (2014). Necrotic cell death in Caenorhabditis
1070 elegans. *Methods in enzymology*, *545*, 127–155. https://doi.org/10.1016/B978-0-12-801430-
1071 1.00006-8
1072 83. Nordquist, S. K., Smith, S. R., and Pierce, J. T. (2018). Systematic Functional
1073 Characterization of Human 21st Chromosome Orthologs in *Caenorhabditis elegans*. *G3*
1074 *(Bethesda, Md.)*, *8*(3), 967–979. https://doi.org/10.1534/g3.118.200019
1075 84. Nuriel, T., Angulo, S. L., Khan, U., Ashok, A., Chen, Q., Figueroa, H. Y., Emrani, S., Liu, L.,
1076 Herman, M., Barrett, G., Savage, V., Buitrago, L., Cepeda-Prado, E., Fung, C., Goldberg, E.,
1077 Gross, S. S., Hussaini, S. A., Moreno, H., Small, S. A., and Duff, K. E. (2017). Neuronal

1078 hyperactivity due to loss of inhibitory tone in APOE4 mice lacking Alzheimer's disease-like
1079 pathology. *Nature communications*, *8*(1), 1464. https://doi.org/10.1038/s41467-017-01444-0
1080 85. Oakley, S. S., Maina, M. B., Marshall, K. E., Al-Hilaly, Y. K., Harrington, C. R., Wischik, C.
1081 M., and Serpell, L. C. (2020). Tau Filament Self-Assembly and Structure: Tau as a
1082 Therapeutic Target. *Frontiers in neurology*, *11*, 590754.
1083 https://doi.org/10.3389/fneur.2020.590754
1084 86. O'Hagan, R., Chalfie, M., and Goodman, M. B. (2005). The MEC-4 DEG/ENaC channel of
1085 Caenorhabditis elegans touch receptor neurons transduces mechanical signals. *Nature*
1086 *neuroscience*, *8*(1), 43–50. https://doi.org/10.1038/nn1362
1087 87. Pan CL, Peng CY, Chen CH, McIntire S. Genetic analysis of age-dependent defects of the
1088 Caenorhabditis elegans touch receptor neurons. Proc Natl Acad Sci U S A. 2011 May
1089 31;108(22):9274-9. doi: 10.1073/pnas.1011711108. Epub 2011 May 12. PMID: 21571636;
1090 PMCID: PMC3107274.
1091 88. Rietdijk, C. D., Perez-Pardo, P., Garssen, J., van Wezel, R. J., and Kraneveld, A. D. (2017).
1092 Exploring Braak's Hypothesis of Parkinson's Disease. *Frontiers in neurology*, *8*, 37.
1093 https://doi.org/10.3389/fneur.2017.00037
1094 89. Roberson, E. D., Scearce-Levie, K., Palop, J. J., Yan, F., Cheng, I. H., Wu, T., Gerstein, H.,
1095 Yu, G. Q., and Mucke, L. (2007). Reducing endogenous tau ameliorates amyloid beta-
1096 induced deficits in an Alzheimer's disease mouse model. *Science (New York, N.Y.)*,
1097 *316*(5825), 750–754. https://doi.org/10.1126/science.1141736
1098 90. Robinson, J. L., Lee, E. B., Xie, S. X., Rennert, L., Suh, E., Bredenberg, C., Caswell, C.,
1099 Van Deerlin, V. M., Yan, N., Yousef, A., Hurtig, H. I., Siderowf, A., Grossman, M., McMillan,
1100 C. T., Miller, B., Duda, J. E., Irwin, D. J., Wolk, D., Elman, L., McCluskey, L., … Trojanowski,
1101 J. Q. (2018). Neurodegenerative disease concomitant proteinopathies are prevalent, age-
1102 related and APOE4-associated. *Brain : a journal of neurology*, *141*(7), 2181–2193.
1103 https://doi.org/10.1093/brain/awy146
1104 91. Rohn, T. T., Catlin, L. W., Coonse, K. G., and Habig, J. W. (2012). Identification of an
1105 amino-terminal fragment of apolipoprotein E4 that localizes to neurofibrillary tangles of the
1106 Alzheimer's disease brain. *Brain research*, *1475*, 106–115.
1107 https://doi.org/10.1016/j.brainres.2012.08.003
1108 92. Rondina, J. M., Ferreira, L. K., de Souza Duran, F. L., Kubo, R., Ono, C. R., Leite, C. C.,
1109 Smid, J., Nitrini, R., Buchpiguel, C. A., and Busatto, G. F. (2017). Selecting the most
1110 relevant brain regions to discriminate Alzheimer's disease patients from healthy controls
1111 using multiple kernel learning: A comparison across functional and structural imaging
1112 modalities and atlases. *NeuroImage. Clinical*, *17*, 628–641.
1113 https://doi.org/10.1016/j.nicl.2017.10.026

1114 93. Rosen, H. J., Allison, S. C., Schauer, G. F., Gorno-Tempini, M. L., Weiner, M. W., and Miller,
1115 B. L. (2005). Neuroanatomical correlates of behavioural disorders in dementia. *Brain : a*
1116 *journal of neurology*, *128*(Pt 11), 2612–2625. https://doi.org/10.1093/brain/awh628
1117 94. Roux, A. E., Yuan, H., Podshivalova, K., Hendrickson, D., Kerr, R., Kenyon, C., and Kelley,
1118 D. (2023). Individual cell types in C. elegans age differently and activate distinct cell-
1119 protective responses. *Cell reports*, *42*(8), 112902.
1120 https://doi.org/10.1016/j.celrep.2023.112902
1121 95. Ryan, N. S., and Rossor, M. N. (2010). Correlating familial Alzheimer's disease gene
1122 mutations with clinical phenotype. *Biomarkers in medicine*, *4*(1), 99–112.
1123 https://doi.org/10.2217/bmm.09.92
1124 96. Sae-Lee, W., Scott, L. L., Brose, L., Encarnacion, A. J., Shi, T., Kore, P., Oyibo, L. O., Ye,
1125 C., Rozmiarek, S. K., and Pierce, J. T. (2020). *APP*-Induced Patterned Neurodegeneration
1126 Is Exacerbated by *APOE4* in *Caenorhabditis elegans*. *G3 (Bethesda, Md.)*, *10*(8), 2851–
1127 2861. https://doi.org/10.1534/g3.120.401486
1128 97. Sanfeliu-Cerdán, N., Català-Castro, F., Mateos, B., Garcia-Cabau, C., Ribera, M., Ruider, I.,
1129 Porta-de-la-Riva, M., Canals-Calderón, A., Wieser, S., Salvatella, X., and Krieg, M. (2023).
1130 A MEC-2/stomatin condensate liquid-to-solid phase transition controls neuronal
1131 mechanotransduction during touch sensing. *Nature cell biology*, *25*(11), 1590–1599.
1132 https://doi.org/10.1038/s41556-023-01247-0
1133 98. Santarella, R. A., Skiniotis, G., Goldie, K. N., Tittmann, P., Gross, H., Mandelkow, E. M.,
1134 Mandelkow, E., and Hoenger, A. (2004). Surface-decoration of microtubules by human tau.
1135 *Journal of molecular biology*, *339*(3), 539–553. https://doi.org/10.1016/j.jmb.2004.04.008
1136 99. Scahill, R. I., Schott, J. M., Stevens, J. M., Rossor, M. N., and Fox, N. C. (2002). Mapping
1137 the evolution of regional atrophy in Alzheimer's disease: unbiased analysis of fluid-
1138 registered serial MRI. *Proceedings of the National Academy of Sciences of the United*
1139 *States of America*, *99*(7), 4703–4707. https://doi.org/10.1073/pnas.052587399
1140 100. Schafer W. R. (2005). Egg-laying. *WormBook : the online review of C. elegans biology*,
1141 1–7. https://doi.org/10.1895/wormbook.1.38.1
1142 101. Scharf, A., Pohl, F., Egan, B. M., Kocsisova, Z., and Kornfeld, K. (2021). Reproductive
1143 Aging in *Caenorhabditis elegans*: From Molecules to Ecology. *Frontiers in cell and*
1144 *developmental biology*, *9*, 718522. https://doi.org/10.3389/fcell.2021.718522
1145 102. Schneider, C. A., Rasband, W. S., and Eliceiri, K. W. (2012). NIH Image to ImageJ: 25
1146 years of image analysis. *Nature Methods*, *9*(7), 671–675. doi:10.1038/nmeth.2089
1147 103. Seo, D. O., O'Donnell, D., Jain, N., Ulrich, J. D., Herz, J., Li, Y., Lemieux, M., Cheng, J.,
1148 Hu, H., Serrano, J. R., Bao, X., Franke, E., Karlsson, M., Meier, M., Deng, S., Desai, C.,
1149 Dodiya, H., Lelwala-Guruge, J., Handley, S. A., Kipnis, J., … Holtzman, D. M. (2023). ApoE

1150 isoform- and microbiota-dependent progression of neurodegeneration in a mouse model of
1151 tauopathy. *Science (New York, N.Y.)*, *379*(6628), eadd1236.
1152 https://doi.org/10.1126/science.add1236
1153 104. Serrano-Pozo, A., Das, S., and Hyman, B. T. (2021). APOE and Alzheimer's disease:
1154 advances in genetics, pathophysiology, and therapeutic approaches. *The Lancet.*
1155 *Neurology*, *20*(1), 68–80. https://doi.org/10.1016/S1474-4422(20)30412-9
1156 105. Shi, Y., Yamada, K., Liddelow, S. A., Smith, S. T., Zhao, L., Luo, W., Tsai, R. M., Spina,
1157 S., Grinberg, L. T., Rojas, J. C., Gallardo, G., Wang, K., Roh, J., Robinson, G., Finn, M. B.,
1158 Jiang, H., Sullivan, P. M., Baufeld, C., Wood, M. W., Sutphen, C., … Holtzman, D. M.
1159 (2017). ApoE4 markedly exacerbates tau-mediated neurodegeneration in a mouse model of
1160 tauopathy. *Nature*, *549*(7673), 523–527. https://doi.org/10.1038/nature24016
1161 106. Spittaels, K., Van den Haute, C., Van Dorpe, J., Bruynseels, K., Vandezande, K.,
1162 Laenen, I., Geerts, H., Mercken, M., Sciot, R., Van Lommel, A., Loos, R., and Van Leuven,
1163 F. (1999). Prominent axonopathy in the brain and spinal cord of transgenic mice
1164 overexpressing four-repeat human tau protein. *The American journal of pathology*, *155*(6),
1165 2153–2165. https://doi.org/10.1016/S0002-9440(10)65533-2
1166 107. Steciuk, M., Cheong, M., Waite, C., You, Y. J., and Avery, L. (2014). Regulation of
1167 synaptic transmission at the Caenorhabditis elegans M4 neuromuscular junction by an
1168 antagonistic relationship between two calcium channels. *G3 (Bethesda, Md.)*, *4*(12), 2535–
1169 2543. https://doi.org/10.1534/g3.114.014308
1170 108. Strang, K. H., Golde, T. E., and Giasson, B. I. (2019). MAPT mutations, tauopathy, and
1171 mechanisms of neurodegeneration. *Laboratory investigation; a journal of technical methods*
1172 *and pathology*, *99*(7), 912–928. https://doi.org/10.1038/s41374-019-0197-x
1173 109. Sündermann, F., Fernandez, M. P., and Morgan, R. O. (2016). An evolutionary roadmap
1174 to the microtubule-associated protein MAP Tau. *BMC genomics*, *17*, 264.
1175 https://doi.org/10.1186/s12864-016-2590-9
1176 110. Taylor, S. R., Santpere, G., Weinreb, A., Barrett, A., Reilly, M. B., Xu, C., Varol, E.,
1177 Oikonomou, P., Glenwinkel, L., McWhirter, R., Poff, A., Basavaraju, M., Rafi, I., Yemini, E.,
1178 Cook, S. J., Abrams, A., Vidal, B., Cros, C., Tavazoie, S., Sestan, N., … Miller, D. M., 3rd
1179 (2021). Molecular topography of an entire nervous system. *Cell*, *184*(16), 4329–4347.e23.
1180 https://doi.org/10.1016/j.cell.2021.06.023
1181 111. Therriault, J., Benedet, A. L., Pascoal, T. A., Mathotaarachchi, S., Chamoun, M., Savard,
1182 M., Thomas, E., Kang, M. S., Lussier, F., Tissot, C., Parsons, M., Qureshi, M. N. I., Vitali, P.,
1183 Massarweh, G., Soucy, J. P., Rej, S., Saha-Chaudhuri, P., Gauthier, S., and Rosa-Neto, P.
1184 (2020). Association of Apolipoprotein E ε4 With Medial Temporal Tau Independent of
1185 Amyloid-β. *JAMA neurology*, *77*(4), 470–479. https://doi.org/10.1001/jamaneurol.2019.4421

1186 112. Topalidou, I., Chen, P. A., Cooper, K., Watanabe, S., Jorgensen, E. M., and Ailion, M.
1187 (2017). The NCA-1 and NCA-2 Ion Channels Function Downstream of G_q and Rho To
1188 Regulate Locomotion in *Caenorhabditis elegans*. *Genetics*, *206*(1), 265–282.
1189 https://doi.org/10.1534/genetics.116.198820
1190 113. Trent, C., Tsung, N., and Horvitz, H. R. (1983). Egg-laying defective mutants of the
1191 nematode Caenorhabditis elegans. *Genetics*, *104*(4), 619–647.
1192 https://doi.org/10.1093/genetics/104.4.619
1193 114. Trent, C., Tsung, N., and Horvitz, H. R. (1983). Egg-laying defective mutants of the
1194 nematode Caenorhabditis elegans. *Genetics*, *104*(4), 619–647.
1195 https://doi.org/10.1093/genetics/104.4.619
1196 115. Treusch, S., Hamamichi, S., Goodman, J. L., Matlack, K. E., Chung, C. Y., Baru, V.,
1197 Shulman, J. M., Parrado, A., Bevis, B. J., Valastyan, J. S., Han, H., Lindhagen-Persson, M.,
1198 Reiman, E. M., Evans, D. A., Bennett, D. A., Olofsson, A., DeJager, P. L., Tanzi, R. E.,
1199 Caldwell, K. A., Caldwell, G. A., … Lindquist, S. (2011). Functional links between Aβ toxicity,
1200 endocytic trafficking, and Alzheimer's disease risk factors in yeast. *Science (New York,*
1201 *N.Y.)*, *334*(6060), 1241–1245. https://doi.org/10.1126/science.1213210
1202 116. Trojanowski, J. Q., Schmidt, M. L., Shin, R. W., Bramblett, G. T., Rao, D., and Lee, V. M.
1203 (1993). Altered tau and neurofilament proteins in neuro-degenerative diseases: diagnostic
1204 implications for Alzheimer's disease and Lewy body dementias. *Brain pathology (Zurich,*
1205 *Switzerland)*, *3*(1), 45–54. https://doi.org/10.1111/j.1750-3639.1993.tb00725.x
1206 117. Tsutsui, K., Kim, H. S., Yoshikata, C., Kimura, K., Kubota, Y., Shibata, Y., Tian, C., Liu,
1207 J., and Nishiwaki, K. (2021). Repulsive guidance molecule acts in axon branching in
1208 Caenorhabditis elegans. *Scientific reports*, *11*(1), 22370. https://doi.org/10.1038/s41598-
1209 021-01853-8
1210 118. Tuovinen, T., Kananen, J., Rajna, Z., Lieslehto, J., Korhonen, V., Rytty, R., Mattila, H.,
1211 Huotari, N., Raitamaa, L., Helakari, H., Elseoud, A. A., Krüger, J., LeVan, P., Tervonen, O.,
1212 Hennig, J., Remes, A. M., Nedergaard, M., and Kiviniemi, V. (2020). The variability of
1213 functional MRI brain signal increases in Alzheimer's disease at cardiorespiratory
1214 frequencies. *Scientific reports*, *10*(1), 21559. https://doi.org/10.1038/s41598-020-77984-1
1215 119. Vaccaro, A., Tauffenberger, A., Aggad, D., Rouleau, G., Drapeau, P., and Parker, J. A.
1216 (2012). Mutant TDP-43 and FUS cause age-dependent paralysis and neurodegeneration in
1217 C. elegans. *PloS one*, *7*(2), e31321. https://doi.org/10.1371/journal.pone.0031321
1218 120. van Ham, T. J., Thijssen, K. L., Breitling, R., Hofstra, R. M., Plasterk, R. H., and Nollen,
1219 E. A. (2008). C. elegans model identifies genetic modifiers of alpha-synuclein inclusion
1220 formation during aging. *PLoS genetics*, *4*(3), e1000027.
1221 https://doi.org/10.1371/journal.pgen.1000027

121. Vidal-Gadea, A., Topper, S., Young, L., Crisp, A., Kressin, L., Elbel, E., Maples, T., Brauner, M., Erbguth, K., Axelrod, A., Gottschalk, A., Siegel, D., and Pierce-Shimomura, J. T. (2011). Caenorhabditis elegans selects distinct crawling and swimming gaits via dopamine and serotonin. *Proceedings of the National Academy of Sciences of the United States of America*, *108*(42), 17504–17509. https://doi.org/10.1073/pnas.1108673108

122. Vogel, J. W., Iturria-Medina, Y., Strandberg, O. T., Smith, R., Levitis, E., Evans, A. C., Hansson, O., Alzheimer's Disease Neuroimaging Initiative, and Swedish BioFinder Study (2020). Spread of pathological tau proteins through communicating neurons in human Alzheimer's disease. *Nature communications*, *11*(1), 2612. https://doi.org/10.1038/s41467-020-15701-2

123. Vogel, J. W., Iturria-Medina, Y., Strandberg, O. T., Smith, R., Levitis, E., Evans, A. C., Hansson, O., Alzheimer's Disease Neuroimaging Initiative, and Swedish BioFinder Study (2020). Spread of pathological tau proteins through communicating neurons in human Alzheimer's disease. *Nature communications*, *11*(1), 2612. https://doi.org/10.1038/s41467-020-15701-2

124. Vossel, K. A., Zhang, K., Brodbeck, J., Daub, A. C., Sharma, P., Finkbeiner, S., Cui, B., and Mucke, L. (2010). Tau reduction prevents Abeta-induced defects in axonal transport. *Science (New York, N.Y.)*, *330*(6001), 198. https://doi.org/10.1126/science.1194653

125. Way, J. C., and Chalfie, M. (1989). The mec-3 gene of Caenorhabditis elegans requires its own product for maintained expression and is expressed in three neuronal cell types. *Genes & development*, *3*(12A), 1823–1833. https://doi.org/10.1101/gad.3.12a.1823

126. Wegmann, S., Maury, E. A., Kirk, M. J., Saqran, L., Roe, A., DeVos, S. L., Nicholls, S., Fan, Z., Takeda, S., Cagsal-Getkin, O., William, C. M., Spires-Jones, T. L., Pitstick, R., Carlson, G. A., Pooler, A. M., and Hyman, B. T. (2015). Removing endogenous tau does not prevent tau propagation yet reduces its neurotoxicity. *The EMBO journal*, *34*(24), 3028–3041. https://doi.org/10.15252/embj.201592748

127. White, J. G., Southgate, E., Thomson, J. N., and Brenner, S. (1986). The structure of the nervous system of the nematode Caenorhabditis elegans. *Philosophical transactions of the Royal Society of London. Series B, Biological sciences*, *314*(1165), 1–340. https://doi.org/10.1098/rstb.1986.0056

128. Wu, Z., Cardona, E. A., Cohn, J. A., and Pierce, J. T. (2025). Nonapoptotic role of EGL-1 in exopher production and neuronal health in *Caenorhabditis elegans*. *Proceedings of the National Academy of Sciences of the United States of America*, *122*(2), e2407909122. https://doi.org/10.1073/pnas.2407909122

129. Wu, Z., Ghosh-Roy, A., Yanik, M. F., Zhang, J. Z., Jin, Y., and Chisholm, A. D. (2007). Caenorhabditis elegans neuronal regeneration is influenced by life stage, ephrin signaling,

and synaptic branching. *Proceedings of the National Academy of Sciences of the United States of America*, *104*(38), 15132–15137. https://doi.org/10.1073/pnas.0707001104

130. Yoshiyama, Y., Higuchi, M., Zhang, B., Huang, S. M., Iwata, N., Saido, T. C., Maeda, J., Suhara, T., Trojanowski, J. Q., and Lee, V. M. (2007). Synapse loss and microglial activation precede tangles in a P301S tauopathy mouse model. *Neuron*, *53*(3), 337–351. https://doi.org/10.1016/j.neuron.2007.01.010

131. Zhou, W., Scott, S. A., Shelton, S. B., and Crutcher, K. A. (2006). Cathepsin D-mediated proteolysis of apolipoprotein E: possible role in Alzheimer's disease. *Neuroscience*, *143*(3), 689–701. https://doi.org/10.1016/j.neuroscience.2006.08.019

Figure captions MAIN

Fig. 1.
Deletion of *ptl-1* partially suppresses progressive pattern of behavioral decline induced by APOE4

(A left) Timeline to the adult age of onset of defective or abnormal behaviors in APOE4 strain.
(A right) Endogenous *ptl-1* locus with all known isoforms and the portion deleted in the *ok621* allele as indicated below.
(B-H) Results of behavioral assays, used to proxy neuronal dysfunction, are arranged by the age of onset for APOE4-induced defects. Only in the cases of gentle touch sensation and pumping behaviors (B,C) are APOE4 defects suppressed such that there are no significant differences between control and APOE4;Δ*ptl-1* groups.
(B-E) D1 adult onset. (B) Subtle defect in gentle touch sensitivity which is fully suppressed by *ptl-1* deletion. N=47 for control, N=30 for Δ*ptl-1*, N=33 for APOE4, and N=35 for APOE4;Δ*ptl-1*. (C) Subtle defect in pharyngeal pumping which is fully suppressed by *ptl-1* deletion. N=94 for control, N=37 for Δ*ptl-1*, N=61 for APOE4, and N=91 for APOE4;Δ*ptl-1*. (D) Severe defect in swim-to-crawl gait transition which is partially suppressed by *ptl-1* deletion. N=164 control, N=136 for Δ*ptl-1*, N=162 for APOE4, N=165 for APOE4;Δ*ptl-1*. (E) Subtle defect in short-term locomotion which is not suppressed by *ptl-1* deletion. N=47 for control, N=38 for Δ*ptl-1*, N=44 for APOE4, and N=44 for APOE4;Δ*ptl-1*.
(F) D2 adult onset. Subtle defect in long-term locomotion was not suppressed by *ptl-1* deletion. N=31 control, N=32 for Δ*ptl-1*, N=28 for APOE4, and N=29 for APOE4;Δ*ptl-1*.
(G,H) D3 adult onset. (G) Severe egg laying defect was partially suppressed by *ptl-1* deletion. N=196 for control, N=134 for Δ*ptl-1*, N=214 for APOE4, N=243 for APOE4;Δ*ptl-1*. (H) Subtle, abnormal increase in harsh touch sensitivity. N=25 for control, N=17 for Δ*ptl-1*, N=26 for APOE4, and N=31 for APOE4;Δ*ptl-1*.
All data are represented as mean ± SEM. N is the total sample size representing all animals across replicates. Statistical comparisons were made using χ^2 tests of independence for D,G and planned tests after two-way ANOVA for B,C,E,F,G. *: $p<0.05$; **: $p<0.01$; ***: $p<0.001$.

Fig. 2.
APOE4-induced behavioral decline may be the result of developmental and age-related defects

(A,B) Assays of gentle touch sensitivity. (A) Control worms maintained sensitivity from L4 (N=18) to D1 adult (N=22) to D3 adult (N=22) age. (B) APOE4 worms showed a decrease in sensitivity from L4 (N=18) to D1 adult (N=17) and remained unchanged afterward into D3 adult (N=17) age.

1306 (C,D) Assays of pharyngeal pumping. (C) Control worms showed an expected increase in
1307 pumping behavior from L4 (N=18) to D1 adult (N=20) that remained into D3 adult (N=16) age.
1308 (D) APOE4 worms showed no difference in pumping across L4 (N=18) to D1 adult (N=17) to D3
1309 adult (N=20) ages.
1310 All data are represented as mean ± SEM. N is the total sample size. Statistical comparisons
1311 were made using planned tests after two-way ANOVA. *: $p<0.05$; **: $p<0.01$; ***: $p<0.001$.
1312
1313
1314 **Fig. 3**
1315 **Deletion of *ptl-1* partially suppresses APOE4-induced HSN axon dysmorphia**
1316 (A) Cartoon of the worm midbody, centered about the vulva area, depicting: the HSN proximal
1317 axon, the VC4,5 neurons, vulval musculature, and ventral nerve cord (VNC). For the proximal
1318 axon: segment i. is the initial, anteriorly projecting portion and segment ii. is the ventrally
1319 projecting portion.
1320 (B) Representative live images of normal (1,2) and abnormal (3-10) HSN proximal axons
1321 visualized with GFP. Proximal axon segments are marked by i. and ii (with exception to image
1322 2, where segment identity is less certain). The vulva area is also marked with a white arrowhead
1323 for anatomical reference. All scale bars are 20 µm.
1324 (C,D) Percentage of animals with abnormal HSN proximal axons in D1 and D3 adults. The
1325 baseline incidence of abnormal axons in control was similar between D1 and D3.
1326 (C) D1 adults. All other groups show non-significant, but slightly increased incidence of
1327 abnormal axons compared to control. N=37 for control, N=59 Δ*ptl-1*, N=51 for APOE4, N=22 for
1328 APOE4;Δ*ptl-1* (left), and N=37 for APOE4;Δ*ptl-1* (right).
1329 (D) The incidence of abnormal axons appears to correlate with defective egg laying behavior
1330 (See Fig. 1G) in D3 adults. N=101 for control, N=78 for Δ*ptl-1*, N=91 for APOE4, N=79 for
1331 APOE4;Δ*ptl-1* (left), and N=86 for APOE4;Δ*ptl-1* (right).
1332 (E,F) Quantification of HSN proximal axon lengths in D1 and D3 adults. The baseline axon
1333 length in control was similar between D1 and D3.
1334 (E) D1 adults. Axon length was similar across all groups. N=15 for control, N=13 Δ*ptl-1*, N=20
1335 for APOE4, N=6 for APOE4;Δ*ptl-1* (left), and N=10 for APOE4;Δ*ptl-1* (right).
1336 (F) D3 adults. Axon length appears to correlate with the incidence of abnormal axons shown in
1337 (C) and defective egg laying behavior (See Fig. 1G). N=79 for control, N=66 for Δ*ptl-1*, N=72 for
1338 APOE4, N=54 for APOE4;Δ*ptl-1* (left), and N=66 for APOE4;*ptl-1* (right).
1339 (G) By-day breakdown of defective egg laying as quantified cumulatively in Fig. 1G. D3 data are
1340 replotted from Fig. 1G.
1341 All data are represented as mean ± SEM. N is the total sample size representing all animals
1342 across replicates. Statistical comparisons were made using χ^2 tests of independence for C and
1343 D and planned comparisons after two-way ANOVAs for E and F. *: $p<0.05$; **: $p<0.01$; ***:
1344 $p<0.001$.
1345
1346
1347 **Fig. 4.**
1348 **Targeted genetic ablation, but not abolished function, of the TRNs protects HSN against**
1349 **APOE4-induced dysfunction**
1350 (A1) Egg-laying behavior across groups. Genetic ablation of the TRNs partially suppressed egg-
1351 laying defects in APOE4 animals as with the *ptl-1* deletion (See Fig. 1G). N=104 for control,
1352 N=171 for TRNs::EGL-1, N=525 for APOE4, and N=190 for APOE4;TRNs::EGL-1.
1353 (A2 top) Cartoon depicting the head and tail areas wherein the nerve ring and PLM neuron,
1354 respectively, are located.
1355 (A2 bottom) Representative live images of nerve ring (arrowhead) and PLM neuron (within
1356 dashed circle if present; marked with asterisk if absent) visualized with PTL-1::mNG in control
1357 and TRNs::EGL-1 animals. Dashed borders indicate the worm body outline. All scale bars are
1358 20 µm.

1359 (B) Egg-laying behavior across groups. In contrast to genetic ablation, abolishing TRN function
1360 did not suppress egg laying defects. N=104 for control, N=123 for *mec-4*(*lf*), N=525 for APOE4,
1361 and N=226 for APOE4;*mec-4*(*lf*).
1362 All data are represented as mean ± SEM. N is the total sample size representing all animals
1363 across replicates. All statistical comparisons were made using χ^2 tests of independence. control
1364 and APOE4 data are re-plotted in A1 and B. *: p<0.05; **: p<0.01; ***: p<0.001.
1365
1366
1367 **Fig. 5.**
1368 **Targeted depletion of PTL-1 in the TRNs protects HSN against APOE4-induced**
1369 **dysfunction**
1370 (A1) Egg-laying behavior across groups. N=104 for control, N=180 for TRNs::*ptl-1* KD, N=525
1371 for APOE4, N=171 for APOE4;TRNs::*ptl-1* KD (left), and N=108 for APOE4;TRNs::*ptl-1* KD
1372 (right).
1373 (A2) Quantification of *ptl-1* knockdown in the targeted TRNs and non-targeted VCs4,5 neurons
1374 between control and TRNs::*ptl-1* KD animals using PTL-1::mNG fluorescence intensity in the
1375 soma.
1376 (B1) Egg-laying behavior across groups. N=104 for control, N=348 for TRNs::*ptl-1* KO, N=525
1377 for APOE4, N=423 for APOE4;TRNs:: *ptl-1* KO (left), and N=519 for APOE4;TRNs:: *ptl-1* KO
1378 (right).
1379 (B2) Representative live images of nerve ring (arrowhead) and PLM neuron (within dashed
1380 circle if present; area marked with asterisk if absent) visualized with PTL-1::mNG in control and
1381 TRNs::*ptl-1* KO animals. Dashed borders indicate the worm body outline. All scale bars are 20
1382 µm.
1383 (B3) Percentage of animals with abnormal HSN proximal axons in D3 adults using independent
1384 reporter transgenics from Fig. 3. N=31 for TRNs::*ptl-1* KO and N=17 for APOE4;TRNs::*ptl-1* KO.
1385 (C) Egg-laying behavior across groups. N=104 for control, N=80 for CHEs::*ptl-1* KO, N=525 for
1386 APOE4, and N=78 for APOE4;TRNs:: *ptl-1* KO.
1387 All data are represented as mean ± SEM. N is the total sample size representing all animals
1388 across replicates. Statistical comparisons were made using χ^2 tests of independence for
1389 A1,B1,B3,C and Student's t-test for A2. Control and APOE4 data are re-plotted in A1, B1, and
1390 C. *: p<0.05; **: p<0.01; ***: p<0.001.
1391
1392

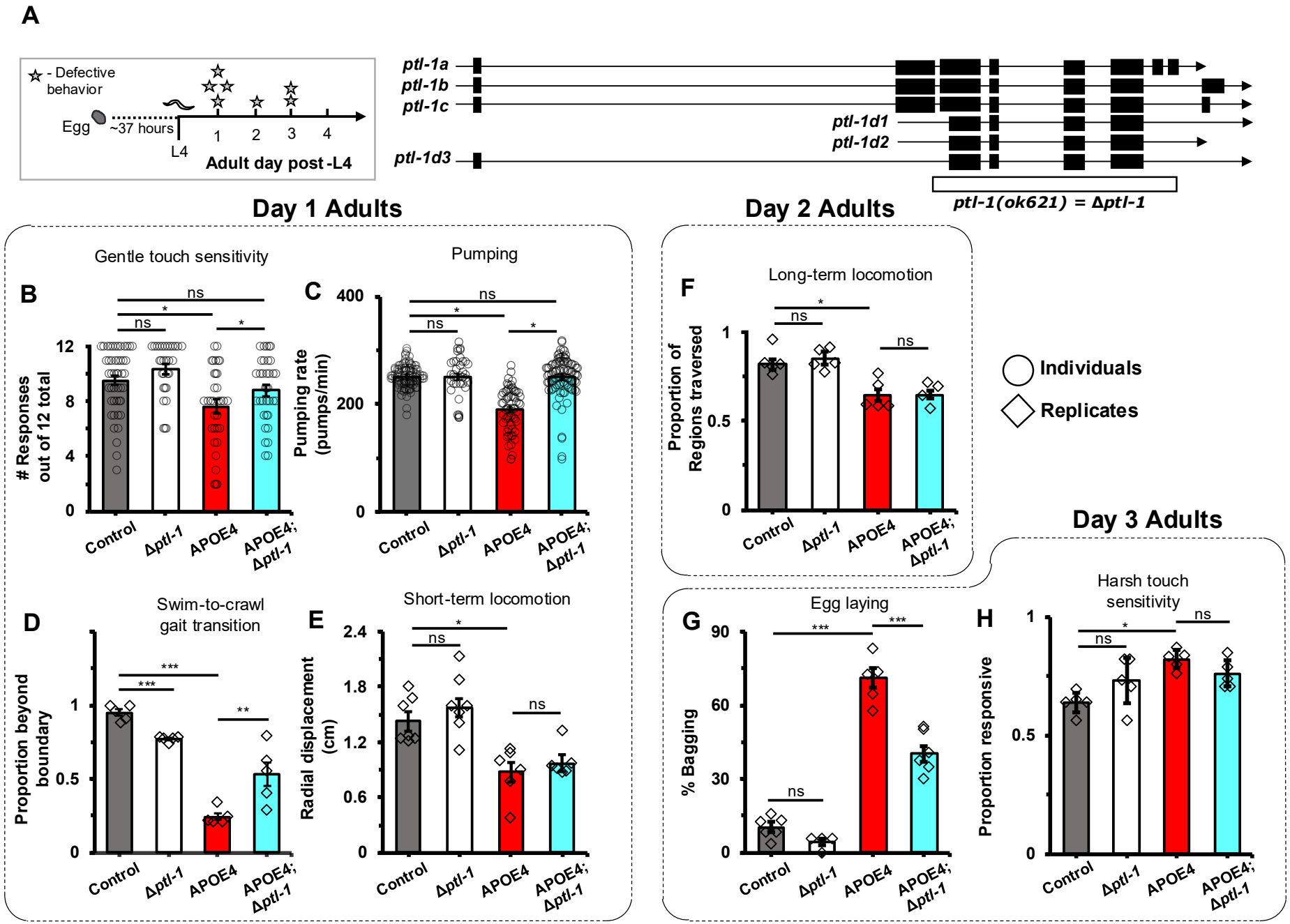
A
- Defective behavior
Egg
~37 hours
L4
1
2
3
4
Adult day post -L4
ptl-1a
ptl-1b
ptl-1c
ptl-1d1
ptl-1d2
ptl-1d3
ptl-1(ok621) = Δptl-1
Day 1 Adults
Gentle touch sensitivity
B
Responses out of 12 total
Pumping
C
Pumping rate (pumps/min)
Swim-to-crawl gait transition
D
Proportion beyond boundary
Short-term locomotion
E
Radial displacement (cm)
Day 2 Adults
Long-term locomotion
F
Proportion of Regions traversed
Individuals
Replicates
Day 3 Adults
Egg laying
G
% Bagging
Harsh touch sensitivity
H
Proportion responsive
Control
Δptl-1
APOE4
APOE4; Δptl-1
ns
*
**
***

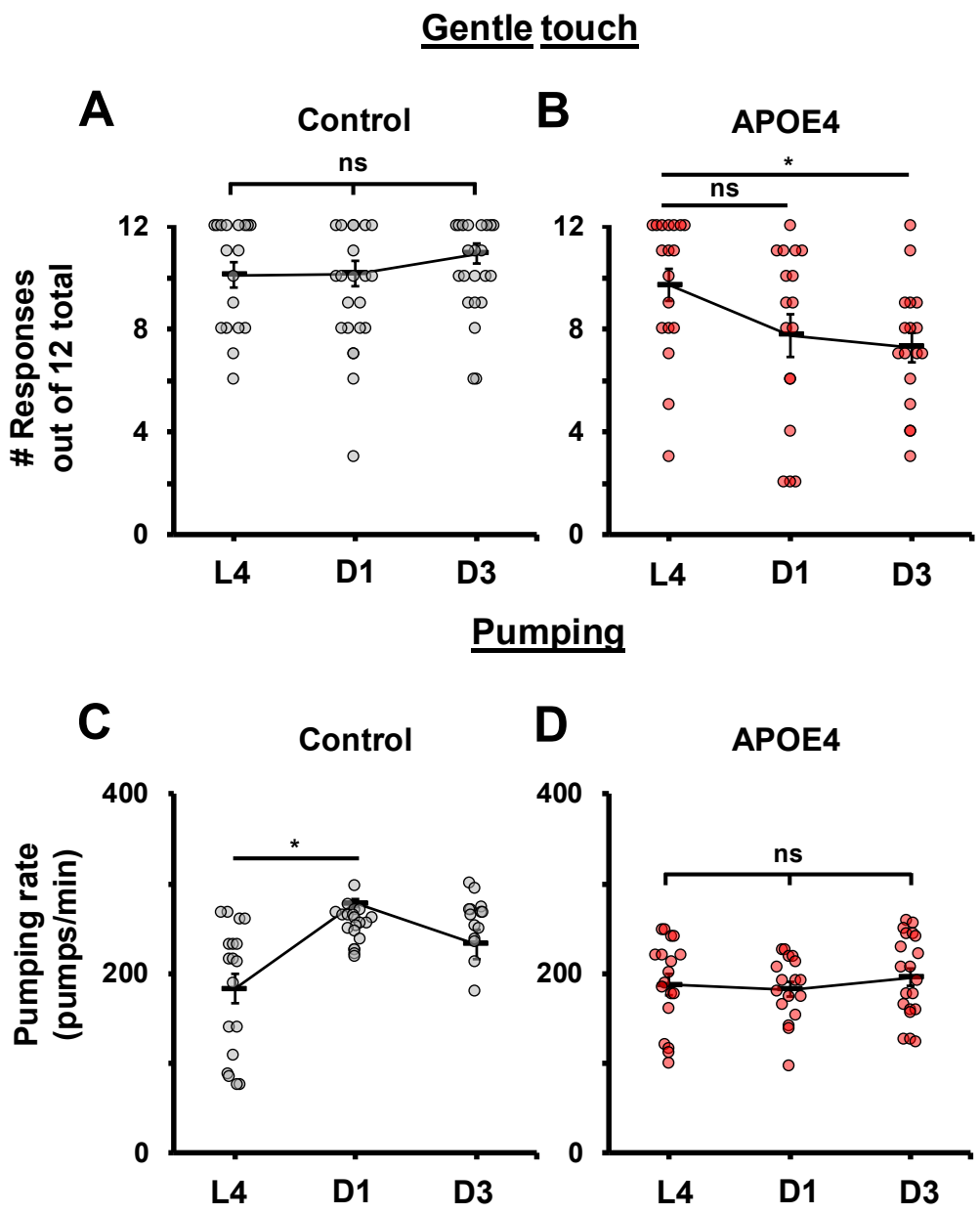
Gentle touch
A
Control
ns
B
APOE4
*
ns
Responses
out of 12 total
12
8
4
0
L4
D1
D3
Pumping
C
Control
*
D
APOE4
ns
Pumping rate
(pumps/min)
400
200
0
L4
D1
D3

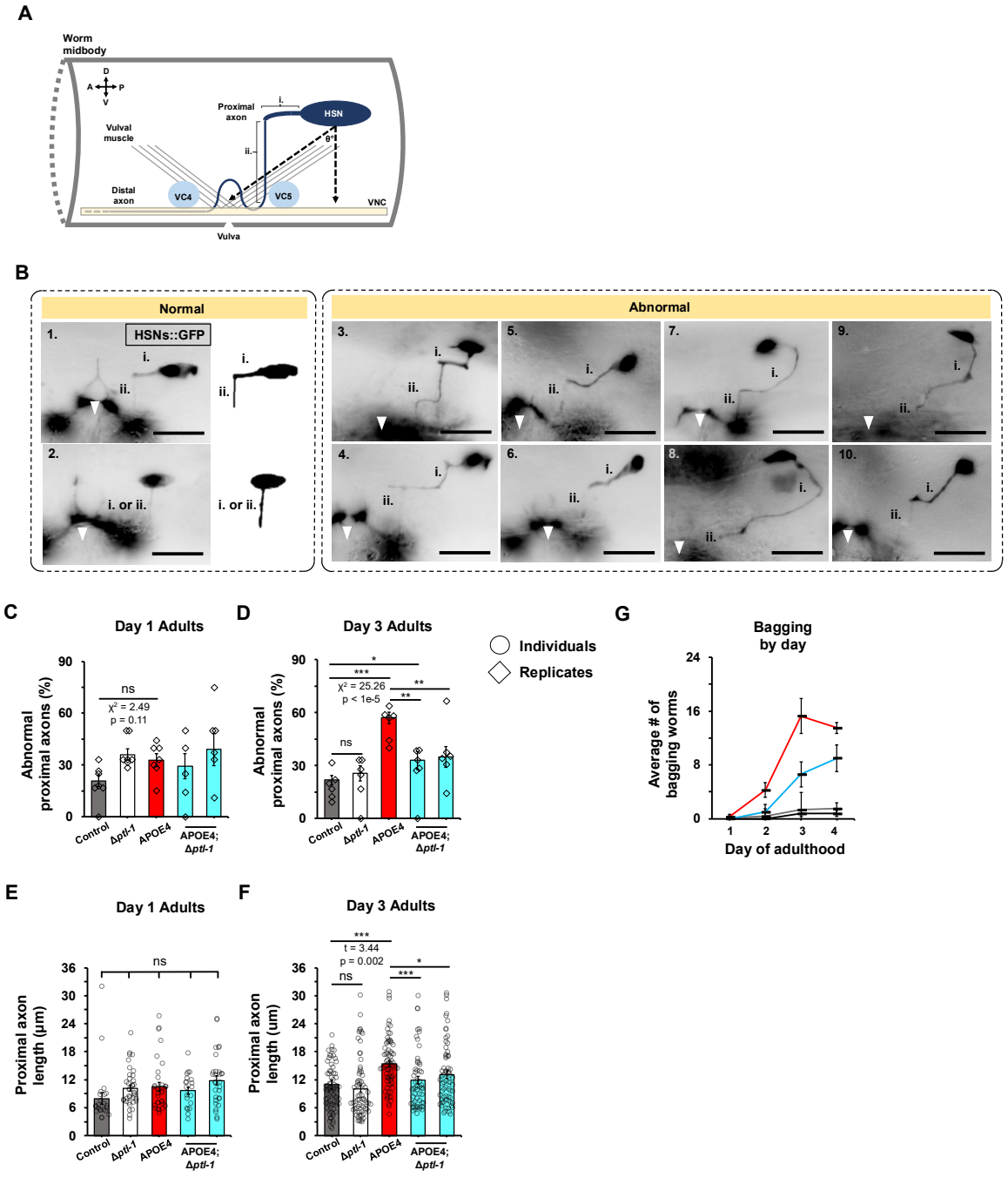
A
Worm midbody
D
A
P
V
Proximal axon
i.
HSN
Vulval muscle
ii.
Distal axon
VC4
VC5
VNC
Vulva
B
Normal
Abnormal
HSNs::GFP
1.
2.
3.
4.
5.
6.
7.
8.
9.
10.
i.
ii.
i. or ii.
C
Day 1 Adults
Abnormal proximal axons (%)
ns
χ² = 2.49
p = 0.11
Control
Δptl-1
APOE4
APOE4; Δptl-1
D
Day 3 Adults
Abnormal proximal axons (%)
*
***
χ² = 25.26
p < 1e-5
**
ns
Individuals
Replicates
G
Bagging by day
Average # of bagging worms
Day of adulthood
E
Day 1 Adults
Proximal axon length (µm)
ns
F
Day 3 Adults
Proximal axon length (um)
***
t = 3.44
p = 0.002
ns
*
***

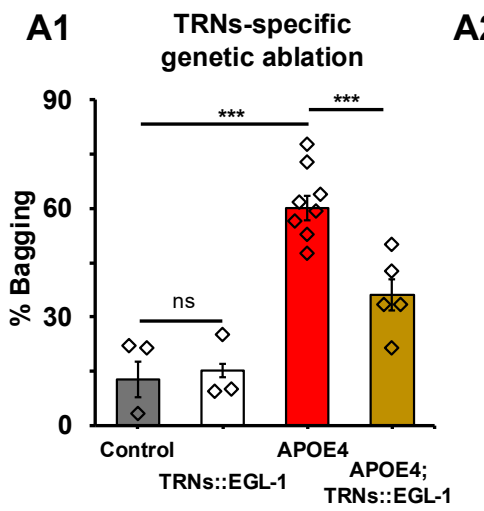
A1
TRNs-specific genetic ablation
% Bagging
90
60
30
0
***
***
ns
Control
TRNs::EGL-1
APOE4
APOE4; TRNs::EGL-1

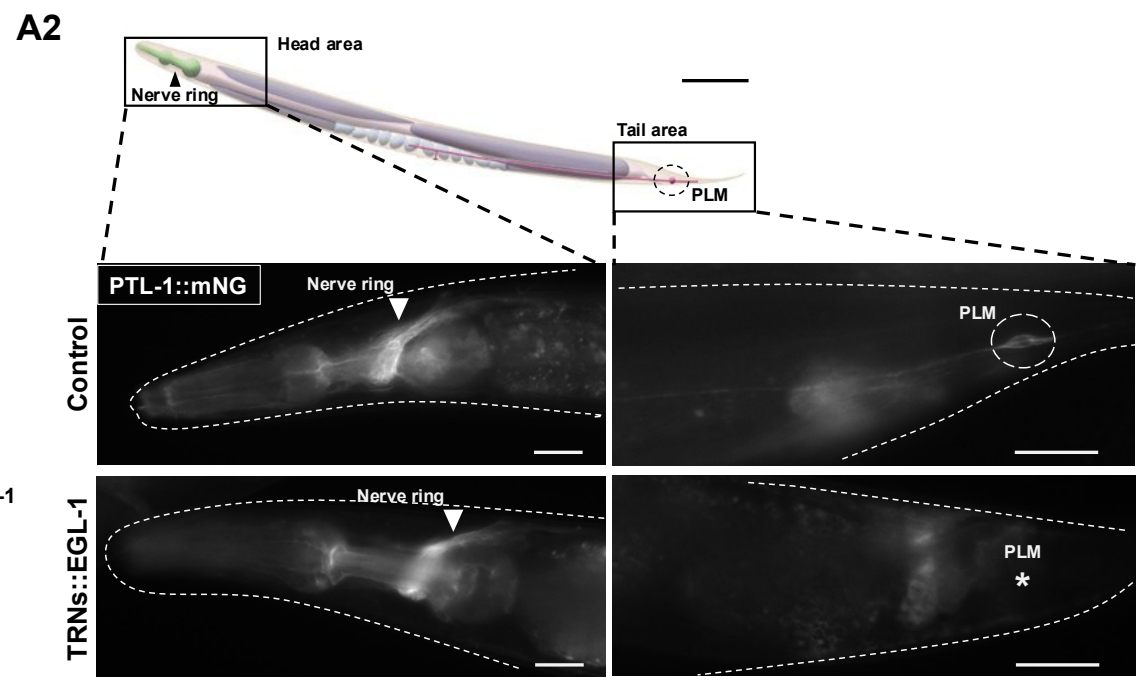
A2
Head area
Nerve ring
Tail area
PLM
PTL-1::mNG
Nerve ring
PLM
Control
Nerve ring
PLM
*
TRNs::EGL-1

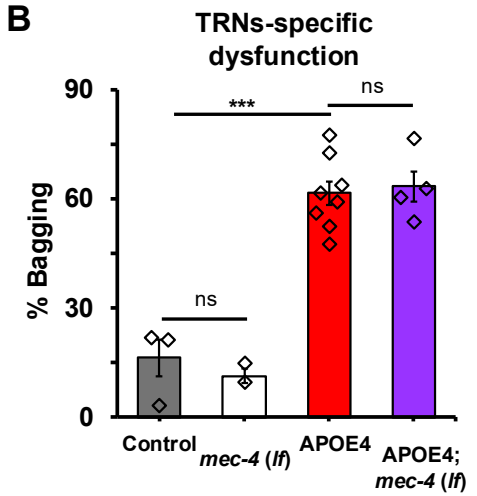
B
TRNs-specific dysfunction
% Bagging
90
60
30
0
***
ns
ns
Control
mec-4 (lf)
APOE4
APOE4; mec-4 (lf)

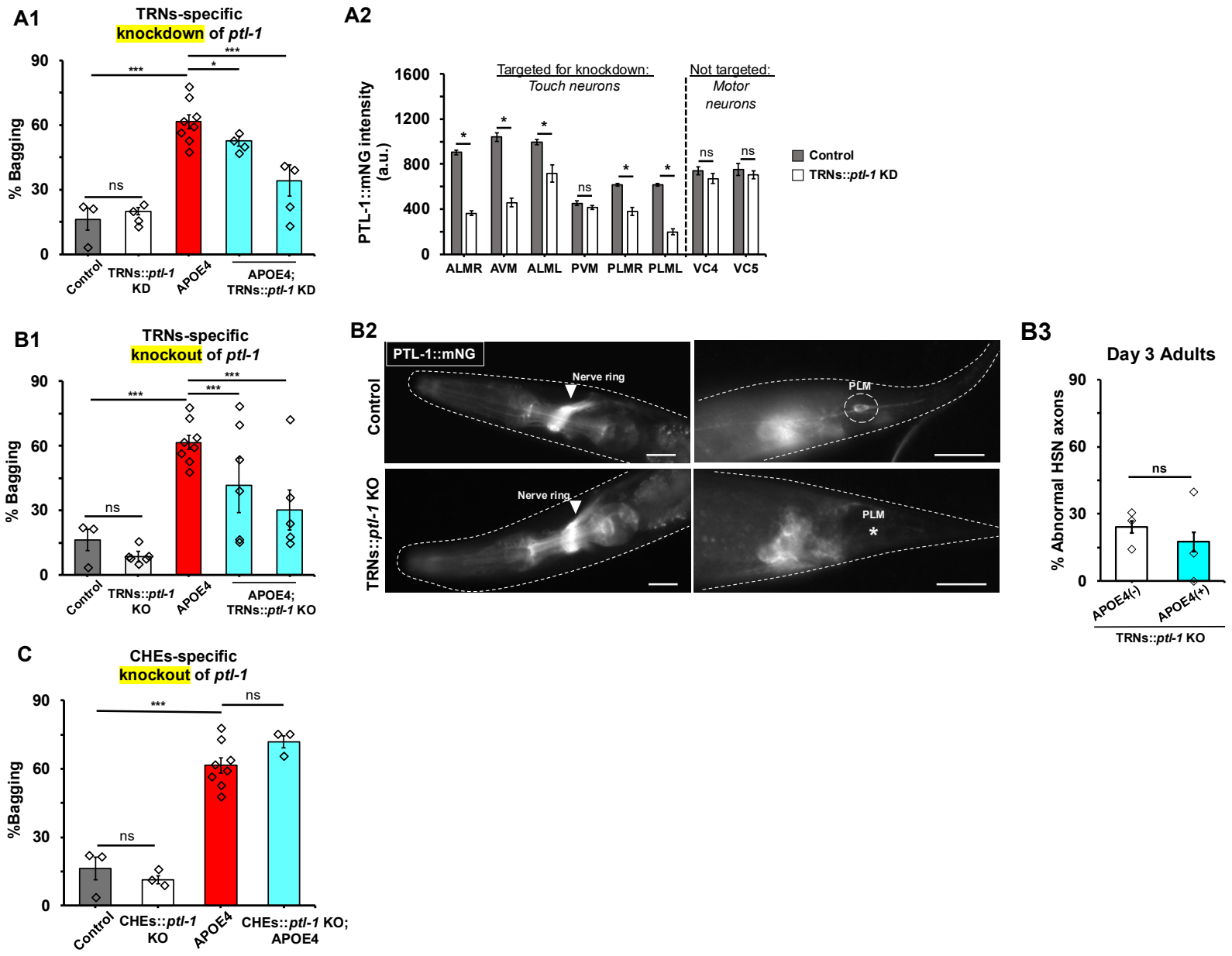
A1
TRNs-specific knockdown of ptl-1
% Bagging
90
60
30
0
***
*
***
ns
Control
TRNs::ptl-1 KD
APOE4
APOE4; TRNs::ptl-1 KD
A2
PTL-1::mNG intensity (a.u.)
1600
1200
800
400
0
Targeted for knockdown: Touch neurons
Not targeted: Motor neurons
ALMR
AVM
ALML
PVM
PLMR
PLML
VC4
VC5
Control
TRNs::ptl-1 KD
B1
TRNs-specific knockout of ptl-1
% Bagging
TRNs::ptl-1 KO
APOE4; TRNs::ptl-1 KO
B2
PTL-1::mNG
Nerve ring
PLM
Control
TRNs::ptl-1 KO
B3
Day 3 Adults
% Abnormal HSN axons
APOE4(-)
APOE4(+)
TRNs::ptl-1 KO
C
CHEs-specific knockout of ptl-1
%Bagging
CHEs::ptl-1 KO
CHEs::ptl-1 KO; APOE4